PHYSICS LETTERS B

Observation of the Higgs boson decay to a pair of τ leptons with the CMS detector

The CMS Collaboration[*]

CERN, Switzerland

ARTICLE INFO

ABSTRACT

A measurement of the H $\to \tau\tau$ signal strength is performed using events recorded in proton–proton collisions by the CMS experiment at the LHC in 2016 at a center-of-mass energy of 13 TeV. The data set corresponds to an integrated luminosity of 35.9 fb^{-1}. The H $\to \tau\tau$ signal is established with a significance of 4.9 standard deviations, to be compared to an expected significance of 4.7 standard deviations. The best fit of the product of the observed H $\to \tau\tau$ signal production cross section and branching fraction is $1.09^{+0.27}_{-0.26}$ times the standard model expectation. The combination with the corresponding measurement performed with data collected by the CMS experiment at center-of-mass energies of 7 and 8 TeV leads to an observed significance of 5.9 standard deviations, equal to the expected significance. This is the first observation of Higgs boson decays to τ leptons by a single experiment.

1. Introduction

In the standard model (SM) of particle physics [1–3], electroweak symmetry breaking is achieved via the Brout–Englert–Higgs mechanism [4–9], leading, in its minimal version, to the prediction of the existence of one physical neutral scalar particle, commonly known as the Higgs boson (H). A particle compatible with such a boson was observed by the ATLAS and CMS experiments at the CERN LHC in the ZZ, $\gamma\gamma$, and W$^+$W$^-$ decay channels [10–12], during the proton–proton (pp) data taking period in 2011 and 2012 at center-of-mass energies of $\sqrt{s} = 7$ and 8 TeV, respectively. Subsequent results from both experiments, described in Refs. [13–18], established that the measured properties of the new particle, including its spin, CP properties, and coupling strengths to SM particles, are consistent with those expected for the Higgs boson predicted by the SM. The mass of the Higgs boson has been determined to be 125.09 ± 0.21 (stat) ± 0.11 (syst) GeV, from a combination of ATLAS and CMS measurements [19].

To establish the mass generation mechanism for fermions, it is necessary to probe the direct coupling of the Higgs boson to such particles. The most promising decay channel is $\tau^+\tau^-$, because of the large event rate expected in the SM compared to the $\mu^+\mu^-$ decay channel ($\mathcal{B}(\text{H} \to \tau^+\tau^-) = 6.3\%$ for a mass of 125.09 GeV),

and of the smaller contribution from background events with respect to the b$\bar{\text{b}}$ decay channel.

Searches for a Higgs boson decaying to a τ lepton pair were performed at the LEP [20–23], Tevatron [24,25], and LHC colliders. Using pp collision data at $\sqrt{s} = 7$ and 8 TeV, the CMS Collaboration showed evidence for this process with an observed (expected) significance of 3.2 (3.7) standard deviations (s.d.) [26]. The ATLAS experiment reported evidence for Higgs bosons decaying into pairs of τ leptons with an observed (expected) significance of 4.5 (3.4) s.d. for a Higgs boson mass of 125 GeV [27]. The combination of the results from both experiments yields an observed (expected) significance of 5.5 (5.0) s.d. [28].

This Letter reports on a measurement of the H $\to \tau\tau$ signal strength. The analysis targets both the gluon fusion and the vector boson fusion production mechanisms. The analyzed data set corresponds to an integrated luminosity of 35.9 fb^{-1}, and was collected in 2016 in pp collisions at a center-of-mass energy of 13 TeV. In the following, the symbol ℓ refers to electrons or muons, the symbol τ_{h} refers to τ leptons reconstructed in their hadronic decays, and H $\to \tau^+\tau^-$ and H $\to$ W$^+$W$^-$ are simply denoted as H $\to \tau\tau$ and H $\to$ WW, respectively. All possible $\tau\tau$ final states are studied, except for those with two muons or two electrons because of the low branching fraction and large background contribution. The analysis covers about 94% of all possible $\tau\tau$ final states.

2. The CMS detector

The central feature of the CMS apparatus is a superconducting solenoid of 6 m internal diameter, providing a magnetic field of 3.8 T. Within the solenoid volume, there are a silicon pixel and strip tracker, a lead tungstate crystal electromagnetic calorimeter (ECAL), and a brass and scintillator hadron calorimeter (HCAL), each composed of a barrel and two endcap sections. Forward calorimeters extend the pseudorapidity coverage provided by the barrel and endcap detectors. Muons are detected in gas-ionization chambers embedded in the steel flux-return yoke outside the solenoid.

Events of interest are selected using a two-tiered trigger system [29]. The first level (L1), composed of custom hardware processors, uses information from the calorimeters and muon detectors to select events at a rate of around 100 kHz within a time interval of less than 4 μs. The second level, known as the high-level trigger (HLT), consists of a farm of processors running a version of the full event reconstruction software optimized for fast processing, and reduces the event rate to about 1 kHz before data storage.

Significant upgrades of the L1 trigger during the first long shutdown of the LHC have benefited this analysis, especially in the $\tau_h \tau_h$ channel. These upgrades improved the τ_h identification at L1 by giving more flexibility to object isolation, allowing new techniques to suppress the contribution from additional pp interactions per bunch crossing, and to reconstruct the L1 τ_h object in a fiducial region that matches more closely that of a true hadronic τ decay. The flexibility is achieved by employing high bandwidth optical links for data communication and large field-programmable gate arrays (FPGAs) for data processing.

A more detailed description of the CMS detector, together with a definition of the coordinate system used and the relevant kinematic variables, can be found in Ref. [30].

3. Simulated samples

Signal and background processes are modeled with samples of simulated events. The signal samples with a Higgs boson produced through gluon fusion (ggH), vector boson fusion (VBF), or in association with a W or Z boson (WH or ZH), are generated at next-to-leading order (NLO) in perturbative quantum chromodynamics (pQCD) with the POWHEG 2.0 [31–35] generator. The MINLO HVJ [36] extension of POWHEG 2.0 is used for the WH and ZH simulated samples. The set of parton distribution functions (PDFs) is NNPDF30_nlo_as_0118 [37]. The tt̄H process is negligible. The various production cross sections and branching fractions for the SM Higgs boson production, and their corresponding uncertainties, are taken from Refs. [38–40] and references therein.

The MG5_aMC@NLO [41] generator is used for Z + jets and W + jets processes. They are simulated at leading order (LO) with the MLM jet matching and merging [42]. The MG5_aMC@NLO generator is also used for diboson production simulated at next-to-LO (NLO) with the FxFx jet matching and merging [43], whereas POWHEG 2.0 and 1.0 are used for tt̄ and single top quark production, respectively. The generators are interfaced with PYTHIA 8.212 [44] to model the parton showering and fragmentation, as well as the decay of the τ leptons. The PYTHIA parameters affecting the description of the underlying event are set to the CUETP8M1 tune [45].

Generated events are processed through a simulation of the CMS detector based on GEANT4 [46], and are reconstructed with the same algorithms used for data. The simulated samples include additional pp interactions per bunch crossing, referred to as "pileup". The effect of pileup is taken into account by generating concurrent minimum bias collision events generated with PYTHIA. The

simulated events are weighted such that the distribution of the number of additional pileup interactions, estimated from the measured instantaneous luminosity for each bunch crossing, matches that in data, with an average of approximately 27 interactions per bunch crossing.

4. Event reconstruction

The reconstruction of observed and simulated events relies on the particle-flow (PF) algorithm [47], which combines the information from the CMS subdetectors to identify and reconstruct the particles emerging from pp collisions: charged hadrons, neutral hadrons, photons, muons, and electrons. Combinations of these PF objects are used to reconstruct higher-level objects such as jets, τ_h candidates, or missing transverse momentum. The reconstructed vertex with the largest value of summed physics-object p_T^2 is taken to be the primary pp interaction vertex. The physics objects are the objects constructed by a jet finding algorithm [48,49] applied to all charged tracks associated with the vertex, including tracks from lepton candidates, and the corresponding associated missing transverse momentum.

Muons are identified with requirements on the quality of the track reconstruction and on the number of measurements in the tracker and the muon systems [50]. Electrons are identified with a multivariate discriminant combining several quantities describing the track quality, the shape of the energy deposits in the ECAL, and the compatibility of the measurements from the tracker and the ECAL [51]. To reject non-prompt or misidentified leptons, a relative lepton isolation is defined as:

$$I^\ell \equiv \frac{\sum_{\text{charged}} p_T + \max\left(0, \sum_{\text{neutral}} p_T - \frac{1}{2} \sum_{\text{charged, PU}} p_T\right)}{p_T^\ell}. \quad (1)$$

In this expression, $\sum_{\text{charged}} p_T$ is the scalar sum of the transverse momenta of the charged particles originating from the primary vertex and located in a cone of size $\Delta R = \sqrt{(\Delta\eta)^2 + (\Delta\phi)^2} = 0.4$ (0.3) centered on the muon (electron) direction. The sum $\sum_{\text{neutral}} p_T$ represents a similar quantity for neutral particles. The contribution of photons and neutral hadrons originating from pileup vertices is estimated from the scalar sum of the transverse momenta of charged hadrons in the cone originating from pileup vertices, $\sum_{\text{charged, PU}} p_T$. This sum is multiplied by a factor of 1/2, which corresponds approximately to the ratio of neutral to charged hadron production in the hadronization process of inelastic pp collisions, as estimated from simulation. The expression p_T^ℓ stands for the p_T of the lepton. Isolation requirements used in this analysis, based on I^ℓ, are listed in Table 1.

Jets are reconstructed with an anti-k_T clustering algorithm implemented in the FASTJET library [49,52]. It is based on the clustering of neutral and charged PF candidates within a distance parameter of 0.4. Charged PF candidates not associated with the primary vertex of the interaction are not considered when building jets. An offset correction is applied to jet energies to take into account the contribution from additional pp interactions within the same or nearby bunch crossings. The energy of a jet is calibrated based on simulation and data through correction factors [53]. In this analysis, jets are required to have p_T greater than 30 GeV and $|\eta|$ less than 4.7, and are separated from the selected leptons by a ΔR of at least 0.5. The combined secondary vertex (CSV) algorithm is used to identify jets that are likely to originate from a b quark ("b jets"). The algorithm exploits the track-based lifetime information together with the secondary vertices associated with the jet to provide a likelihood ratio discriminator for the b jet identification. A set of p_T-dependent correction factors are applied to

Table 1

Kinematic selection requirements for the four di-τ decay channels. The trigger requirement is defined by a combination of trigger candidates with p_T over a given threshold (in GeV), indicated inside parentheses. The pseudorapidity thresholds come from trigger and object reconstruction constraints. The p_T thresholds for the lepton selection are driven by the trigger requirements, except for the leading τ_h candidate in the $\tau_h\tau_h$ channel, the τ_h candidate in the $\mu\tau_h$ and eτ_h channels, and the muon in the eμ channel, where they have been optimized to increase the significance of the analysis.

Channel	Trigger requirement	Lepton selection		
		p_T (GeV)	η	Isolation
$\tau_h\tau_h$	$\tau_h(35)\,\&\,\tau_h(35)$	$p_T^{\tau_h} > 50\,\&\,40$	$|\eta^{\tau_h}| < 2.1$	MVA τ_h ID
$\mu\tau_h$	$\mu(22)$	$p_T^\mu > 23$ $p_T^{\tau_h} > 30$	$|\eta^\mu| < 2.1$ $|\eta^{\tau_h}| < 2.3$	$I^\mu < 0.15$ MVA τ_h ID
	$\mu(19)\,\&\,\tau_h(21)$	$20 < p_T^\mu < 23$ $p_T^{\tau_h} > 30$	$|\eta^\mu| < 2.1$ $|\eta^{\tau_h}| < 2.3$	$I^\mu < 0.15$ MVA τ_h ID
eτ_h	e(25)	$p_T^e > 26$ $p_T^{\tau_h} > 30$	$|\eta^e| < 2.1$ $|\eta^{\tau_h}| < 2.3$	$I^e < 0.1$ MVA τ_h ID
eμ	e$(12)\,\&\,\mu(23)$	$p_T^e > 13$ $p_T^\mu > 24$	$|\eta^e| < 2.5$ $|\eta^\mu| < 2.4$	$I^e < 0.15$ $I^\mu < 0.2$
	e$(23)\,\&\,\mu(8)$	$p_T^e > 24$ $p_T^\mu > 15$	$|\eta^e| < 2.5$ $|\eta^\mu| < 2.4$	$I^e < 0.15$ $I^\mu < 0.2$

simulated events to account for differences in the b tagging efficiency between data and simulation. The working point chosen in this analysis gives an efficiency for real b jets of about 70%, and for about 1% of light flavor or quark jets being misidentified.

Hadronically decaying τ leptons are reconstructed with the hadron-plus-strips (HPS) algorithm [54,55], which is seeded with anti-k_T jets. The HPS algorithm reconstructs τ_h candidates on the basis of the number of tracks and of the number of ECAL strips in the η–ϕ plane with energy deposits, in the 1-prong, 1-prong $+ \pi^0$(s), and 3-prong decay modes. A multivariate (MVA) discriminator [56], including isolation and lifetime information, is used to reduce the rate for quark- and gluon-initiated jets to be identified as τ_h candidates. The working point used in this analysis has an efficiency of about 60% for genuine τ_h, with about 1% misidentification rate for quark- and gluon-initiated jets, for a p_T range typical of τ_h originating from a Z boson. Electrons and muons misidentified as τ_h candidates are suppressed using dedicated criteria based on the consistency between the measurements in the tracker, the calorimeters, and the muon detectors [54,55]. The working points of these discriminators depend on the decay channel studied. The τ_h energy scale in simulation is corrected per decay mode, on the basis of a measurement in Z $\to \tau\tau$ events. The rate and the energy scale of electrons and muons misidentified as τ_h candidates are also corrected in simulation, on the basis of a tag-and-probe measurement [57] in Z $\to \ell\ell$ events.

All particles reconstructed in the event are used to determine the missing transverse momentum, $\vec{p}_T^{\text{miss}}$. The missing transverse momentum is defined as the negative vectorial sum of the transverse momenta of all PF candidates [58]. It is adjusted for the effect of jet energy corrections. Corrections to the $\vec{p}_T^{\text{miss}}$ are applied to reduce the mismodeling of the simulated Z + jets, W + jets and Higgs boson samples. The corrections are applied to the simulated events on the basis of the vectorial difference of the measured missing transverse momentum and total transverse momentum of neutrinos originating from the decay of the Z, W, or Higgs boson. Their average effect is the reduction of the p_T^{miss} obtained from simulation by a few GeV.

The visible mass of the $\tau\tau$ system, m_{vis}, can be used to separate the H $\to \tau\tau$ signal events from the large contribution of irreducible Z $\to \tau\tau$ events. However, the neutrinos from the τ lepton decays carry a large fraction of the τ lepton energy and reduce the discriminating power of this variable. The SVFIT algorithm combines the $\vec{p}_T^{\text{miss}}$ with the four-vectors of both τ candidates to calculate a more accurate estimate of the mass of the parent bo-

son, denoted as $m_{\tau\tau}$. The resolution of $m_{\tau\tau}$ is between 15 and 20% depending on the $\tau\tau$ final state. A detailed description of the algorithm can be found in Ref. [59]. Both variables are used in the analysis, as detailed in Section 6, and m_{vis} is preferred over $m_{\tau\tau}$ when the background from Z $\to \ell\ell$ events is large.

5. Event selection

Selected events are classified into the various decay channels according to the number of selected electrons, muons, and τ_h candidates. The resulting event samples are made mutually exclusive by discarding events that have additional loosely identified and isolated muons or electrons. Leptons must meet the minimum requirement that the distance of closest approach to the primary vertex satisfies $|d_z| < 0.2$ cm along the beam direction, and $|d_{xy}| < 0.045$ cm in the transverse plane. The two leptons assigned to the Higgs boson decay are required to have opposite-sign electric charges. In the $\mu\tau_h$ channel, events are selected with a combination of online criteria that require at least one isolated muon trigger candidate, or at least one isolated muon and one τ_h trigger candidate, depending on the offline muon p_T. In the eτ_h channel, the trigger system requires at least one isolated electron object, whereas in the eμ channel, the triggers rely on the presence of both an electron and a muon, allowing lower online p_T thresholds. In the $\tau_h\tau_h$ channel, the trigger selects events with two loosely isolated τ_h objects. The selection criteria are summarized in Table 1.

In the $\ell\tau_h$ channels, the large W + jets background is reduced by requiring the transverse mass, m_T, to satisfy

$$m_T \equiv \sqrt{2 p_T^\ell p_T^{\text{miss}} [1 - \cos(\Delta\phi)]} < 50 \text{ GeV}, \qquad (2)$$

where p_T^ℓ is the transverse momentum of the lepton ℓ, and $\Delta\phi$ is the azimuthal angle between its direction and the $\vec{p}_T^{\text{miss}}$.

In the eμ channel, the t$\bar{\text{t}}$ background is reduced by requiring $p_\zeta - 0.85\, p_\zeta^{\text{vis}} > -35$ or -10 GeV depending on the category, where p_ζ is the component of the $\vec{p}_T^{\text{miss}}$ along the bisector of the transverse momenta of the two leptons and p_ζ^{vis} is the sum of the components of the lepton transverse momenta along the same direction [60]. This selection criterion has a high signal efficiency because the $\vec{p}_T^{\text{miss}}$ is typically oriented in the same direction as the visible di-τ system in signal events. In addition, events with a b-tagged jet are discarded to further suppress the t$\bar{\text{t}}$ background in the eμ channel.

Table 2

Category selection and observables used to build the 2D kinematic distributions. The events neither selected in the 0-jet nor in the VBF category are included in the boosted category, as denoted by "Others".

	0-jet	VBF	Boosted
	Selection		
$\tau_h\tau_h$	No jet	≥ 2 jets, $p_T^{\tau\tau} > 100$ GeV, $\Delta\eta_{jj} > 2.5$	Others
$\mu\tau_h$	No jet	≥ 2 jets, $m_{jj} > 300$ GeV, $p_T^{\tau\tau} > 50$ GeV, $p_T^{\tau_h} > 40$ GeV	Others
$e\tau_h$	No jet	≥ 2 jets, $m_{jj} > 300$ GeV, $p_T^{\tau\tau} > 50$ GeV	Others
$e\mu$	No jet	2 jets, $m_{jj} > 300$ GeV	Others
	Observables		
$\tau_h\tau_h$	$m_{\tau\tau}$	$m_{jj}, m_{\tau\tau}$	$p_T^{\tau\tau}, m_{\tau\tau}$
$\mu\tau_h$	τ_h decay mode, m_{vis}	$m_{jj}, m_{\tau\tau}$	$p_T^{\tau\tau}, m_{\tau\tau}$
$e\tau_h$	τ_h decay mode, m_{vis}	$m_{jj}, m_{\tau\tau}$	$p_T^{\tau\tau}, m_{\tau\tau}$
$e\mu$	p_T^{μ}, m_{vis}	$m_{jj}, m_{\tau\tau}$	$p_T^{\tau\tau}, m_{\tau\tau}$

6. Categorization

The event sample is split into three mutually exclusive categories per decay channel. In each category the two variables that maximize the $H \to \tau\tau$ sensitivity are chosen to build two-dimensional (2D) distributions.

The three categories are defined as:

- 0-jet: This category targets Higgs boson events produced via gluon fusion. The two variables chosen to extract the results are m_{vis} and the reconstructed τ_h candidate decay mode (in the $\mu\tau_h$ and $e\tau_h$ decay channels) or the p_T of the muon (in the $e\mu$ channel). The $Z \to \ell\ell$ background is large in the 1-prong and 1-prong$+\pi^0$(s) τ_h decay modes in the $\mu\tau_h$ and $e\tau_h$ channels. The m_{vis} variable is used as a final discriminant in the fit instead of $m_{\tau\tau}$ because it separates the signal from the $Z \to \ell\ell$ background, which peaks around the Z boson mass. The reconstructed τ_h candidate decay mode is used as the other discriminant in the $\mu\tau_h$ and $e\tau_h$ decay channels because the $Z \to \ell\ell$ background is negligible for τ_h reconstructed in the 3-prong decay mode, leading to an increased signal-to-background ratio for this particular decay mode, and several systematic uncertainties related to the τ_h decay mode can be constrained with more precision. The 2D distributions for the signal and $Z \to \ell\ell$ background in the 0-jet category of the $\mu\tau_h$ decay channel are shown in Fig. 1 (top). In the $\tau_h\tau_h$ decay channel, only one observable, $m_{\tau\tau}$, is considered because of the low event yields due to the relatively high p_T thresholds on the τ_h at trigger level, and because of the sharply falling τ_h p_T distribution. Simulations indicate that about 98% of signal events in the 0-jet category correspond to the gluon fusion production mechanism.

- VBF: This category targets Higgs boson events produced via VBF. Events are selected with at least two (exactly two) jets with $p_T > 30$ GeV in the $\tau_h\tau_h$, $\mu\tau_h$, and $e\tau_h$ ($e\mu$) channels. In the $\mu\tau_h$, $e\tau_h$, and $e\mu$ channels, the two leading jets are required to have an invariant mass, m_{jj}, larger than 300 GeV. The variable $p_T^{\tau\tau}$, defined as the magnitude of the vectorial sum of the $\vec{p}_T$ of the visible decay products of the τ leptons and $\vec{p}_T^{miss}$, is required to be greater than 50 (100) GeV in the $\mu\tau_h$ and $e\tau_h$ ($\tau_h\tau_h$) channels to reduce the contribution from W + jets backgrounds. This selection criterion also suppresses the background from SM events composed uniquely of jets produced through the strong interaction, referred to as quantum chromodynamics (QCD) multijet events. In addition, the p_T threshold on the τ_h candidate is raised to 40 GeV in the $\mu\tau_h$ channel, and the two leading jets in the $\tau_h\tau_h$ channel should be separated in pseudorapidity by $\Delta\eta > 2.5$. The two observables in the VBF category are $m_{\tau\tau}$ and m_{jj}. The 2D distributions for the signal and $Z \to \tau\tau$ background in the VBF

category of the $\mu\tau_h$ decay channel are shown in Fig. 1 (center). Integrating over the whole m_{jj} phase space, up to 57% of the signal events in the VBF category are produced in the VBF production mode, but this proportion increases with m_{jj}.

- Boosted: This category contains all the events that do not enter one of the previous categories, namely events with one jet and events with several jets that fail the specific requirements of the VBF category. It contains gluon fusion events produced in association with one or more jets (78–80% of signal events), VBF events where one of the jets has escaped detection or has low m_{jj} (11–13%), as well as Higgs bosons produced in association with a W or a Z boson decaying hadronically (4–8%). While $m_{\tau\tau}$ is chosen as one of the dimensions of the distributions, $p_T^{\tau\tau}$ is taken as the second dimension to specifically target Higgs boson events produced in gluon fusion, with a Lorentz-boosted boson recoiling against jets. Most background processes, including W + jets and QCD multijet events, typically have low $p_T^{\tau\tau}$. The 2D distributions for the signal and W + jets background in the boosted category of the $\mu\tau_h$ decay channel are shown in Fig. 1 (bottom).

The categories and the variables used to build the 2D distributions are summarized in Table 2. The results of the analysis are extracted with a global maximum likelihood fit based on the 2D distributions in the various signal regions, and on some control regions, detailed in Section 7, that constrain the normalizations of the main backgrounds.

7. Background estimation

The largest irreducible source of background is the Drell–Yan production of $Z/\gamma^* \to \tau\tau, \ell\ell$. In order to correct the yield and distributions of the $Z/\gamma^* \to \tau\tau, \ell\ell$ simulations to better reproduce the Drell–Yan process in data, a dedicated control sample of $Z/\gamma^* \to \mu\mu$ events is collected in data with a single-muon trigger, and compared to simulation. The control sample is composed of events with two well-identified and well-isolated opposite-charge muons with p_T greater than 25 GeV and an invariant mass between 70 and 110 GeV. More than 99% of events in this region come from $Z/\gamma^* \to \mu\mu$ decays. Differences in the distributions of $m_{\ell\ell/\tau\tau}$ and $p_T(\ell\ell/\tau\tau)$ in data and in simulations are observed in this control region, and 2D weights based on these variables are derived and applied to simulated $Z/\gamma^* \to \tau\tau, \ell\ell$ events in the signal region of the analysis. In addition, corrections depending on m_{jj} are derived from the $Z/\gamma^* \to \mu\mu$ region and applied to the $Z/\gamma^* \to \tau\tau, \ell\ell$ simulation for events with at least two jets passing the VBF category selection criteria. After this reweighting, good agreement between data in the $Z/\gamma^* \to \mu\mu$ region and simulation is found for all other variables. The simulated sample is split, on the basis of the matching between objects at the generator and
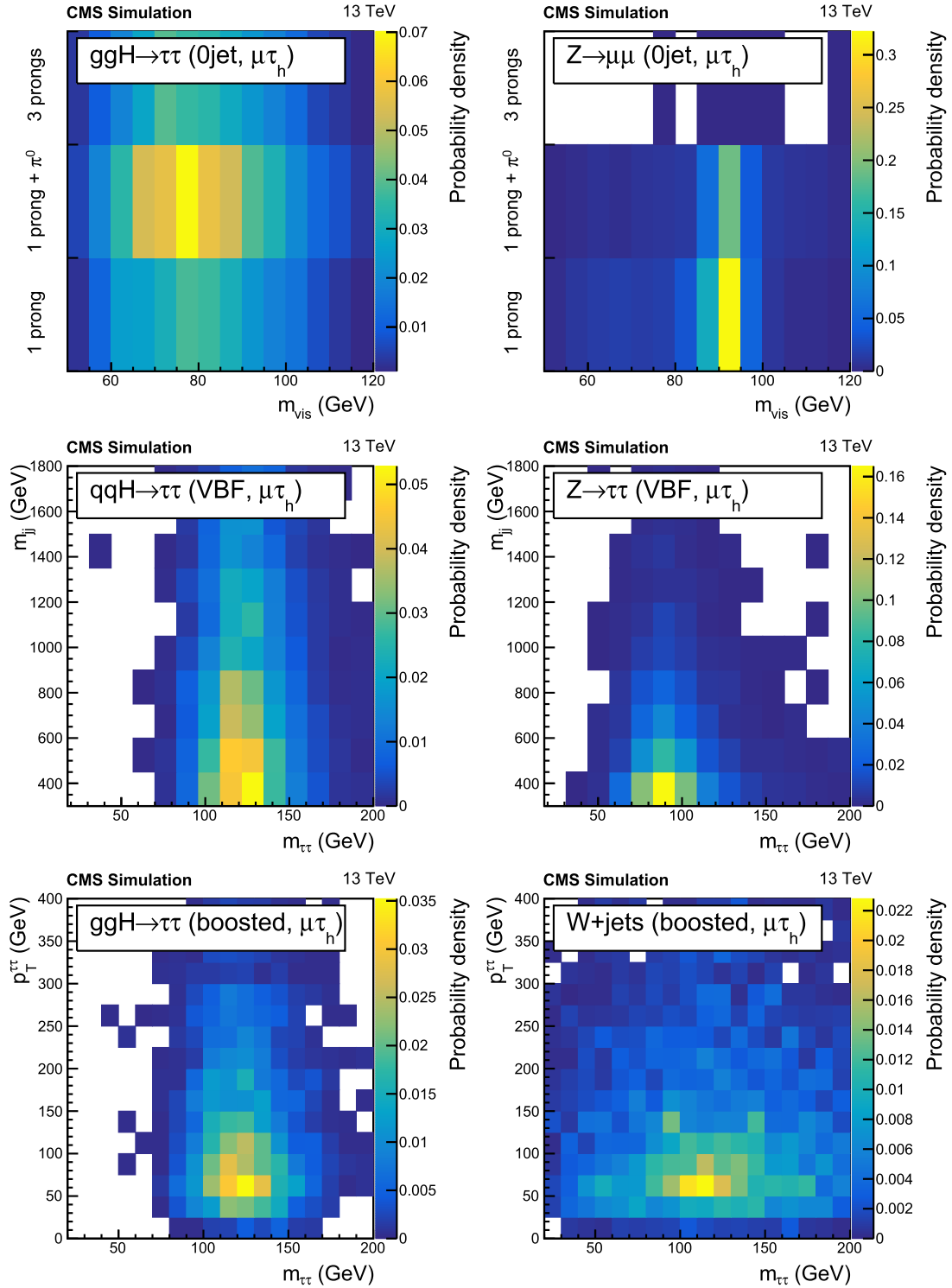
Fig. 1. Distributions for the signal (left) and for some dominant background processes (right) of the two observables chosen in the 0-jet (top), VBF (center), and boosted (bottom) categories in the $\mu\tau_h$ decay channel. The background processes are chosen for illustrative purpose for their separation from the signal. The $Z \to \mu\mu$ background in the 0-jet category is concentrated in the regions where the visible mass is close to 90 GeV and is negligible when the τ_h candidate is reconstructed in the 3-prong decay mode. The $Z \to \tau\tau$ background in the VBF category mostly lies at low m_{jj} values whereas the distribution of VBF signal events extends to high m_{jj} values. In the boosted category, the W+jets background, which behaves similarly to the QCD multijet background, is rather flat with respect to $m_{\tau\tau}$, and is concentrated at low $p_T^{\tau\tau}$ values. These distributions are not used as such to extract the results.
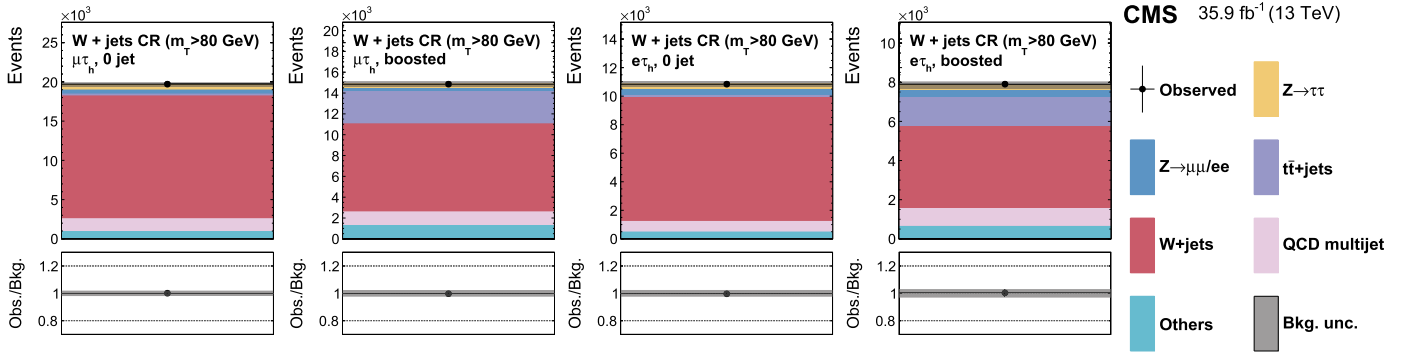
Fig. 2. Control regions enriched in the W + jets background used in the maximum likelihood fit, together with the signal regions, to extract the results. The normalization of the predicted background distributions corresponds to the result of the global fit. These regions, defined with $m_T > 80$ GeV, control the yields of the W + jets background in the $\mu\tau_h$ and $e\tau_h$ channels. The constraints obtained in the boosted categories are propagated to the VBF categories of the corresponding channels.

at the detector levels, into events with prompt leptons (muons or electrons), hadronic decays of the τ leptons, and jets or misidentified objects at the detector level that do not have corresponding objects at generator level within $\Delta R < 0.2$. The electroweak production of Z bosons in association with two jets is also taken into account in the analysis; it contributes up to 8% of the Z boson production in the VBF category.

The background from W + jets production contributes significantly to the $\mu\tau_h$ and $e\tau_h$ channels, when the W boson decays leptonically and a jet is misidentified as a τ_h candidate. The W + jets distributions are modeled using simulation, while their yields are estimated using data, as detailed below. In the boosted and VBF categories, statistical fluctuations in the distributions from simulations are reduced by relaxing the isolation of the τ_h and ℓ candidates, which has been checked not to bias the distributions. The simulated sample is normalized in such a way as to obtain agreement between the yields in data and the predicted backgrounds in a control region enriched in the W + jets background, which is obtained by applying all selection criteria, with the exception that m_T is required to be greater than 80 GeV instead of less than 50 GeV. The W + jets event purity in this region varies from about 50% in the boosted category to 85% in the 0-jet category. The high-m_T sidebands described above, for each category, are considered as control regions in this fit. The constraints obtained in the boosted category are extrapolated to the VBF category of the corresponding decay channel because the topology of the boosted and VBF events is similar, and few data events would pass the high-m_T sideband selection in the VBF category. Fig. 2 shows the control regions with $m_T > 80$ GeV in the 0-jet and boosted categories of the $\mu\tau_h$ and $e\tau_h$ channels. These control regions are composed of only one bin because they are used solely to constrain the normalization of the W + jets process. In the $e\mu$ and $\tau_h\tau_h$ decay channels, the W + jets background is small compared to other backgrounds, and its contribution is estimated from simulations.

The QCD multijet events constitute another important source of reducible background in the $\ell\tau_h$ channels, and it is entirely estimated from data. Various control samples are constituted to estimate the shape and the yield of the QCD multijet background in these channels, as explained below:

1. The raw yield is extracted using a sample where the ℓ and the τ_h candidates have the same sign. Using this sample, the QCD multijet process is estimated from data by subtracting the contribution of the Drell–Yan, $t\bar{t}$, diboson, and W + jets processes.
2. The yield obtained above is corrected to account for differences between the background composition in the same-sign and opposite-sign regions. The extrapolation factor between the same-sign and opposite-sign regions is determined by

comparing the yield of the QCD multijet background for events with ℓ candidates passing inverted isolation criteria, in the same-sign and opposite-sign regions. It is constrained and measured by adding to the global fit the opposite-sign region where the ℓ candidates pass inverted isolation criteria, using the QCD multijet background estimate from the same-sign region with ℓ candidates passing inverted isolation criteria. For the same reasons as in the case of the W + jets background, the constraints are also extrapolated to the VBF signal region. Fig. 3 shows these control regions for the 0-jet and boosted categories of the $\mu\tau_h$ and $e\tau_h$ channels; the observable is m_{vis} or $m_{\tau\tau}$ to provide discrimination between the QCD multijet and the $Z \to \tau\tau$ processes.
3. The 2D distributions of the QCD multijet background are estimated from a region with same-sign leptons, as for the yield estimate, but the isolation of the ℓ and τ_h candidates is additionally relaxed to reduce the statistical fluctuations in the distributions. Again the contribution of the Drell–Yan, $t\bar{t}$, diboson, and W + jets processes are subtracted from data to extract the QCD multijet contribution in this region.

The same technique is used in the $e\mu$ decay channel, but no control region is included in the fit because QCD multijet events contribute little to the total background in this decay channel.

In the $\tau_h\tau_h$ channel, the large QCD multijet background is estimated with a slightly different method, from a sample composed of events with opposite-sign τ_h satisfying a relaxed isolation requirement, disjoint from the signal region. In this region, the QCD multijet background shape and yield are obtained by subtracting the contribution of the Drell–Yan, $t\bar{t}$, and W + jets processes, estimated as explained above, from the data. The QCD multijet background yield in the signal region is obtained by multiplying the yield previously obtained in the control region by an extrapolation factor. The extrapolation factor is measured in events passing identical selection criteria as those in the signal region, and in the relaxed isolation region, except that the τ_h candidates are required to have the same sign. The events selected with opposite-sign τ_h candidates passing relaxed isolation requirements form control regions, shown in Fig. 4, and are used in the fit to extract the results.

The $t\bar{t}$ production process is one of the main backgrounds in the $e\mu$ channel. The 2D distributions in all decay channels are predicted by simulation. The normalization is adjusted to the one observed in a $t\bar{t}$-enriched sample orthogonal to the signal region. This control region, shown in Fig. 5, is added to the global fit to extract the results, and is defined similarly as the $e\mu$ signal region, except that the p_ζ requirement is inverted and the events should contain at least one jet.
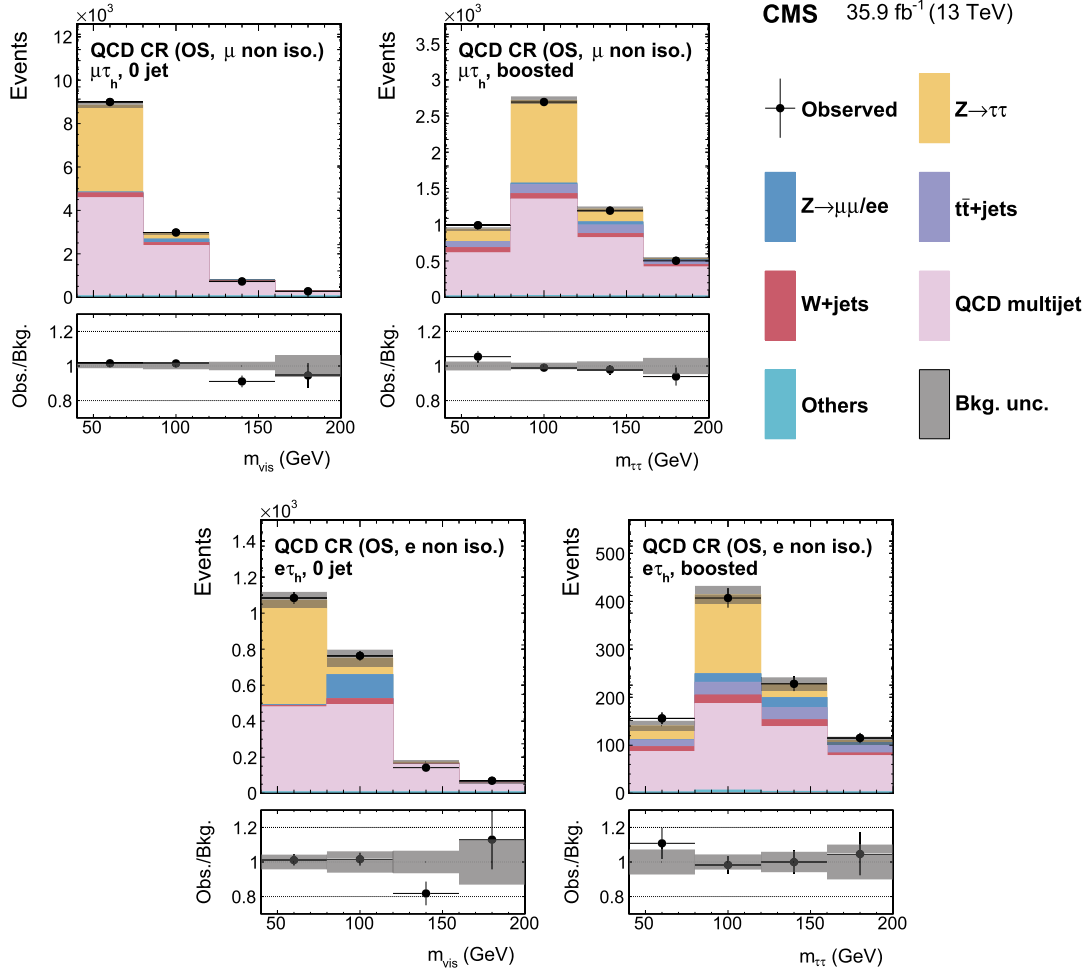
Fig. 3. Control regions enriched in the QCD multijet background used in the maximum likelihood fit, together with the signal regions, to extract the results. The normalization of the predicted background distributions corresponds to the result of the global fit. These regions, defined by selecting events with opposite-sign ℓ and τ_h candidates with ℓ passing inverted isolation conditions, control the yields of the QCD multijet background in the $\mu\tau_h$ and $e\tau_h$ channels. The constraints obtained in the boosted categories are propagated to the VBF categories of the corresponding channels.
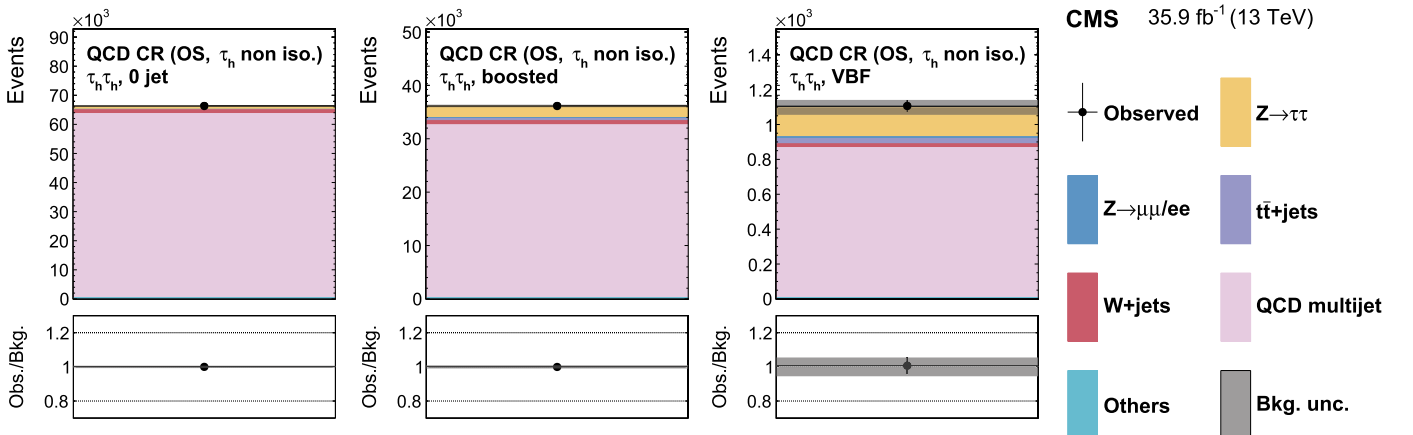
Fig. 4. Control regions enriched in the QCD multijet background used in the maximum likelihood fit, together with the signal regions, to extract the results. The normalization of the predicted background distributions corresponds to the result of the global fit. These regions, formed by selecting events with opposite-sign τ_h candidates passing relaxed isolation requirements, control the yields of the QCD multijet background in the $\tau_h\tau_h$ channel.
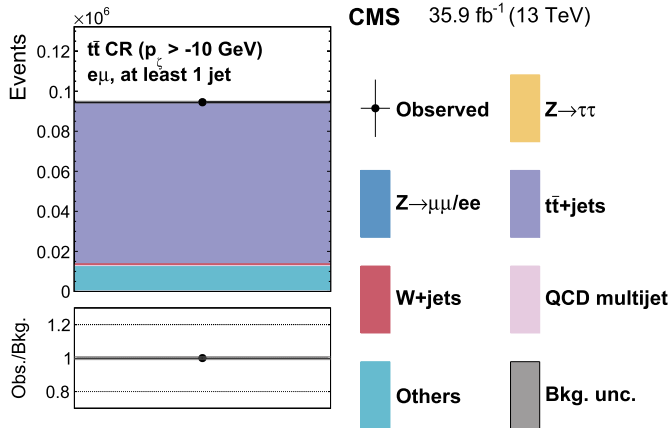
Fig. 5. Control region enriched in the $t\bar{t}$ background, used in the maximum likelihood fit, together with the signal regions, to extract the results. The normalization of the predicted background distributions corresponds to the result of the global fit. This region, defined by inverting the p_ζ requirement and rejecting events with no jet in the $e\mu$ final state, is used to estimate the yields of the $t\bar{t}$ background in all channels.

The contributions from diboson and single top quark production are estimated from simulation, as is the $H \to WW$ background.

8. Systematic uncertainties

8.1. Uncertainties related to object reconstruction and identification

The overall uncertainty in the τ_h identification efficiency for genuine τ_h leptons is 5%, which has been measured with a tag-and-probe method in $Z \to \tau\tau$ events. This number is not fully correlated among the di-τ channels because the τ_h candidates are required to pass different working points of the discriminators that reduce the misidentification rate of electrons and muons as τ_h candidates. The trigger efficiency uncertainty per τ_h candidate amounts to an additional 5%, which leads to a total trigger uncertainty of 10% for processes estimated from simulation in the $\tau_h\tau_h$ decay channel. This uncertainty has also been measured with a tag-and-probe method in $Z \to \tau\tau$ events.

An uncertainty of 1.2% in the visible energy scale of genuine τ_h leptons affects both the distributions and the signal and background yields. It is uncorrelated among the 1-prong, 1-prong$+\pi^0$, and 3-prong decay modes. The magnitude of the uncertainty was determined in $Z \to \tau\tau$ events with one τ lepton decaying hadronically and the other one to a muon, by performing maximum likelihood fits for different values of the visible energy scale of genuine τ_h leptons. Among these events, less than half overlap with the events selected in the $\mu\tau_h$ channel of this analysis. The fit constrains the visible τ_h energy scale uncertainty to about 0.3% for all decay modes. The constraint mostly comes from highly populated regions with a high τ_h purity, namely the 0-jet and boosted categories of the $\mu\tau_h$ and $\tau_h\tau_h$ channels. The decrease in the size of the uncertainty is explained by the addition of two other decay channels with τ_h candidates ($\tau_h\tau_h$ and $e\tau_h$), by the higher number of events in the MC simulations, and by the finer categorization that leads to regions with a high $Z \to \tau\tau$ event purity. Even in the most boosted categories, reconstructed τ_h candidates typically have moderate p_T (p_T less than 100 GeV) and are found in the barrel region of the detector. As tracks are well measured in the CMS detector for this range of p_T, the visible energy scale of genuine τ_h leptons is fully correlated for all τ_h leptons reconstructed in the same decay mode, irrespective of their p_T and η. The uncertainties in the visible energy scale for genuine τ_h leptons together

contribute an uncertainty of 5% to the measurement of the signal strength.

In the 0-jet category of the $\mu\tau_h$ and $e\tau_h$ channels, the relative contribution of τ_h in a given reconstructed decay mode is allowed to fluctuate by 3% to account for the possibility that the reconstruction and identification efficiencies are different for each decay mode. This uncertainty has been measured in a region enriched in $Z \to \tau\tau$ events with one τ lepton decaying hadronically and the other one decaying to a muon, by comparing the level of agreement in exclusive bins of the reconstructed τ_h decay mode, after adjusting the inclusive normalization of the $Z \to \tau\tau$ simulation to its best-fit value. The effect of migration between the reconstructed τ_h decay modes is negligible in other categories, where all decay modes are treated together.

For events where muons or electrons are misidentified as τ_h candidates, essentially $Z \to \mu\mu$ events in the $\mu\tau_h$ decay channel and $Z \to ee$ events in the $e\tau_h$ decay channel, the τ_h identification leads to rate uncertainties of 25 and 12%, respectively, per reconstructed τ_h decay mode. Using m_{vis} and the reconstructed τ_h decay mode as the observables in the 0-jet category of the $\mu\tau_h$ and $e\tau_h$ channels helps reduce the uncertainty after the signal extraction fit: the uncertainty in the rate of muons or electrons misidentified as τ_h becomes of the order of 5%. The energy scale uncertainty for muons or electrons misidentified as τ_h candidates is 1.5 or 3%, respectively, and is uncorrelated between reconstructed τ_h decay modes. The fit constrains these uncertainties to about one third of their initial values. For events where quark- or gluon-initiated jets are misidentified as τ_h candidates, a linear uncertainty that increases by 20% per 100 GeV in τ_h p_T accounts for a potential mismodeling of the jet $\to \tau_h$ misidentification rate as a function of the τ_h p_T in simulations. The uncertainty has been determined from a region enriched in $W + jets$ events, using events with a muon and a τ_h candidate in the final state, characterized by a large transverse mass between the p_T^{miss} and the muon [54,55].

In the decay channels with muons or electrons, the uncertainties in the muon and electron identification, isolation, and trigger efficiencies lead to the rate uncertainty of 2% for both muons and electrons. The uncertainty in the electron energy scale, which amounts to 2.5% in the endcaps and 1% in the barrel of the detector, is relevant only in the $e\mu$ decay channel, where it affects the final distributions. In all channels, the effect of the uncertainty in the muon energy scale is negligible.

The uncertainties in the jet energy scale depend on the p_T and η of the jet [53]. They are propagated to the computation of the number of jets, which affects the repartition of events between the 0-jet, VBF, and boosted categories, and to the computation of m_{jj}, which is one of the observables in the VBF category.

The rate uncertainty related to discarding events with a b-tagged jet in the $e\mu$ decay channel is up to 5% for the $t\bar{t}$ background. The uncertainty in the mistagging rate of gluon and light-flavor jets is negligible.

The $\vec{p}_T^{miss}$ scale uncertainties [61], which are computed event-by-event, affect the normalization of various processes through the event selection, as well as their distributions through the propagation of these uncertainties to the di-τ mass $m_{\tau\tau}$. The $\vec{p}_T^{miss}$ scale uncertainties arising from unclustered energy deposits in the detector come from four independent sources related to the tracker, ECAL, HCAL, and forward calorimeters subdetectors. Additionally, $\vec{p}_T^{miss}$ scale uncertainties related to the uncertainties in the jet energy scale measurement, which lead to uncertainties in the $\vec{p}_T^{miss}$ calculation, are taken into account. The combination of both sources of uncertainties in the $\vec{p}_T^{miss}$ scale leads to an uncertainty of about 10% in the measured signal strength.

8.2. Background estimation uncertainties

The $Z \to \tau\tau$ background yield and distribution are corrected based on the agreement between data and the background prediction in a control region enriched in the $Z \to \mu\mu$ events, as explained in Section 7. The extrapolation uncertainty related to kinematic differences in the selections in the signal and control regions ranges between 3 and 10%, depending on the category. In addition, shape uncertainties related to the uncertainties in the applied corrections are considered; they reach 20% for some ranges of m_{jj} in the VBF category. These uncertainties arise from the different level of agreement between data and simulation in the $Z \to \mu\mu$ control region obtained when varying the threshold on the muon p_T.

The uncertainties in the $W + $ jets event yield determined from the control regions in the $\mu\tau_h$ and $e\tau_h$ channels account for the statistical uncertainty of the observed data, the statistical uncertainty of the $W + $ jets simulated sample, and the systematic uncertainties associated with background processes in these control regions. Additionally, an uncertainty in the extrapolation of the constraints from the high-m_T ($m_T > 80$ GeV) control regions to the low-m_T ($m_T < 50$ GeV) signal regions is additionally taken into account. The latter ranges from 5 to 10%, and is obtained by comparing the m_T distributions of simulated and observed $Z \to \mu\mu$ events where one of the muons is removed and the $\vec{p}_T^{\,miss}$ adjusted accordingly, to mimic $W + $ jets events. The reconstructed invariant mass of the parent boson in the rest frame is multiplied by the ratio of the W and Z boson masses before removing the muon. In the $\tau_h\tau_h$ and $e\mu$ channels, where the $W + $ jets background is estimated from simulation, the uncertainty in the yield of this small background is equal to 4 and 20%, respectively. The larger value for the $e\mu$ channel includes uncertainties in the misidentification rates of jets as electrons and muons, whereas the uncertainty in the misidentification rate of jets as τ_h candidates in the $\tau_h\tau_h$ channel is accounted for by the linear uncertainty as a function of the τ_h p_T described earlier.

The uncertainty in the QCD multijet background yield in the $e\mu$ decay channel ranges from 10 to 20%, depending on the category. It corresponds to the uncertainty in the extrapolation factor from the same-sign to opposite-sign region, measured in events with anti-isolated leptons. In the $\mu\tau_h$ and $e\tau_h$ decay channels, uncertainties from the fit of the control regions with leptons passing relaxed isolation conditions are considered, together with an additional 20% uncertainty that accounts for the extrapolation from the relaxed-isolation control region to the isolated signal region. In the $\tau_h\tau_h$ decay channel, the uncertainty in the QCD mutlijet background yield is a combination of the uncertainties obtained from fitting the dedicated control regions with τ_h candidates passing relaxed isolation criteria, and of extrapolation uncertainties to the signal region ranging from 3 to 15% and accounting for limited disagreement between prediction and data in signal-free regions with various loose isolation criteria.

The yield of events in a $t\bar{t}$-enriched region is added to the maximum likelihood fit to control the normalization of this process in the signal region, as explained in Section 7. The uncertainty from the fit in the control region is automatically propagated to the signal regions, resulting in an uncertainty of about 5% on the $t\bar{t}$ cross section. Per-channel uncertainties related to the object reconstruction and identification are considered when extrapolating from the $e\mu$ final state to the others. The $t\bar{t}$ simulation is corrected for differences in the top quark p_T distributions observed between data and simulation, and an uncertainty in the correction is taken into account.

The combined systematic uncertainty in the background yield arising from diboson and single top quark production processes is estimated to be 5% on the basis of recent CMS measurements [62, 63].

8.3. Signal prediction uncertainties

The rate and acceptance uncertainties for the signal processes related to the theoretical calculations are due to uncertainties in the PDFs, variations of the QCD renormalization and factorization scales, and uncertainties in the modeling of parton showers. The magnitude of the rate uncertainty depends on the production process and on the event category.

The inclusive uncertainty related to the PDFs amounts to 3.2, 2.1, 1.9, and 1.6%, respectively, for the ggH, VBF, WH, and ZH production modes [38]. The corresponding uncertainty for the variation of the renormalization and factorization scales is 3.9, 0.4, 0.7, and 3.8%, respectively [38]. The acceptance uncertainties related to the particular selection criteria used in this analysis are less than 1% for the ggH and VBF productions for the PDF uncertainties. The acceptance uncertainties for the VBF production in the renormalization and factorization scale uncertainties are also less than 1%, while the corresponding uncertainties for the ggH process are treated as shape uncertainties as the uncertainty increases linearly with $p_T^{\tau\tau}$ and m_{jj}.

The p_T distribution of the Higgs boson in the POWHEG 2.0 simulations is tuned to match more closely the next-to-NLO (NNLO) plus next-to-next-to-leading-logarithmic (NNLL) prediction in the HRES2.1 generator [64,65]. The acceptance changes with the variation of the parton shower tune in HERWIG++ 2.6 samples [66] are considered as additional uncertainties, and amount to up to 7% in the boosted category. The theoretical uncertainty in the branching fraction of the Higgs boson to τ leptons is equal to 2.1% [38].

The theoretical uncertainties in the signal production depend on the jet multiplicity; this effect is included by following the prescriptions in Ref. [67]. This effect needs to be taken into account because the definitions of the three categories used in the analysis are based partially on the number of reconstructed jets. Additional uncertainties for boosted Higgs bosons, related to the treatment of the top quark mass in the calculations, are considered for signal events with $p_T^{\tau\tau} > 150$ GeV.

Theory uncertainties in the signal prediction contribute an uncertainty of 10% to the measurement of the signal strength.

8.4. Other uncertainties

The uncertainty in the integrated luminosity amounts to 2.5% [68].

Uncertainties related to the finite number of simulated events, or to the limited number of events in data control regions, are taken into account. They are considered for all bins of the distributions used to extract the results if the uncertainty is larger than 5%. They are uncorrelated across different samples, and across bins of a single distribution. Taken together, they contribute an uncertainty of about 12% to the signal strength measurement, coming essentially from the VBF category, where the background templates are less populated than in the other categories.

The systematic uncertainties considered in the analysis are summarized in Table 3.
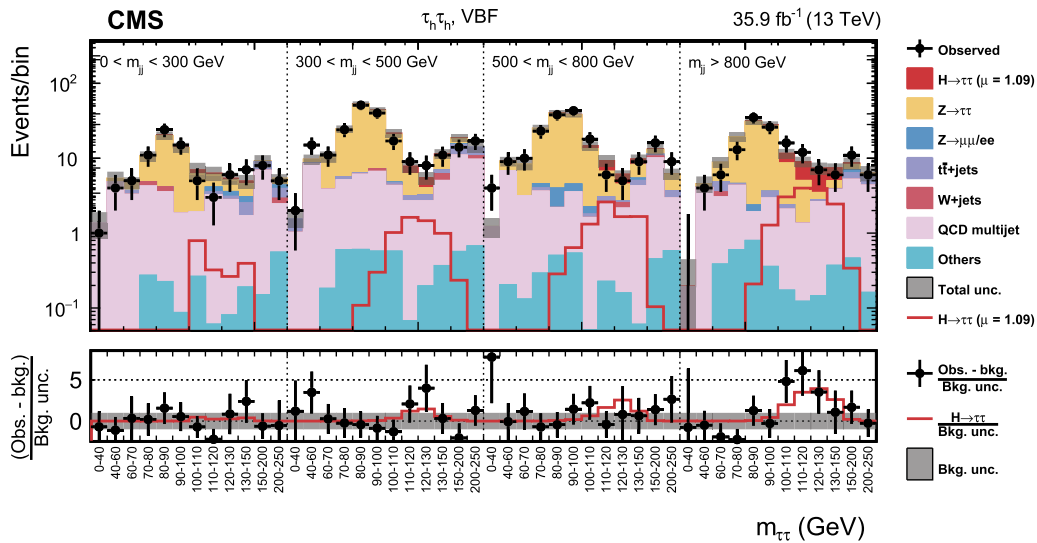
9. Results

The extraction of the results involves a global maximum likelihood fit based on 2D distributions in all channels, shown in Figs. 6–17, together with the control regions for the $t\bar{t}$, QCD multijet, and $W + $ jets backgrounds. The choice of the binning is driven by the statistical precision of the background and data templates,

Table 3

Sources of systematic uncertainty. If the global fit to the signal and control regions, described in the next section, significantly constrains these uncertainties, the values of the uncertainties after the global fit are indicated in the third column. The acronyms CR and ID stand for control region and identification, respectively.

Source of uncertainty	Prefit	Postfit (%)
τ_h energy scale	1.2% in energy scale	0.2–0.3
e energy scale	1–2.5% in energy scale	0.2–0.5
e misidentified as τ_h energy scale	3% in energy scale	0.6–0.8
μ misidentified as τ_h energy scale	1.5% in energy scale	0.3–1.0
Jet energy scale	Dependent upon p_T and η	–
$\vec{p}_T^{\,miss}$ energy scale	Dependent upon p_T and η	–
τ_h ID & isolation	5% per τ_h	3.5
τ_h trigger	5% per τ_h	3
τ_h reconstruction per decay mode	3% migration between decay modes	2
e ID & isolation & trigger	2%	–
μ ID & isolation & trigger	2%	–
e misidentified as τ_h rate	12%	5
μ misidentified as τ_h rate	25%	3–8
Jet misidentified as τ_h rate	20% per 100 GeV τ_h p_T	15
$Z \to \tau\tau/\ell\ell$ estimation	Normalization: 7–15%	3–15
	Uncertainty in $m_{\ell\ell/\tau\tau}$, $p_T(\ell\ell/\tau\tau)$, and m_{jj} corrections	–
W + jets estimation	Normalization (eμ, $\tau_h\tau_h$): 4–20%	–
	Unc. from CR (eτ_h, $\mu\tau_h$): ≃5–15	–
	Extrap. from high-m_T CR (eτ_h, $\mu\tau_h$): 5–10%	–
QCD multijet estimation	Normalization (eμ): 10–20%	5–20%
	Unc. from CR (eτ_h, $\tau_h\tau_h$, $\mu\tau_h$): ≃5–15%	–
	Extrap. from anti-iso. CR (eτ_h, $\mu\tau_h$): 20%	7–10
	Extrap. from anti-iso. CR ($\tau_h\tau_h$): 3–15%	3–10
Diboson normalization	5%	–
Single top quark normalization	5%	–
$t\bar{t}$ estimation	Normalization from CR: ≃5%	–
	Uncertainty on top quark p_T reweighting	–
Integrated luminosity	2.5%	–
b-tagged jet rejection (eμ)	3.5–5.0%	–
Limited number of events	Statistical uncertainty in individual bins	–
Signal theoretical uncertainty	Up to 20%	–

Fig. 6. Observed and predicted 2D distributions in the VBF category of the $\tau_h\tau_h$ decay channel. The normalization of the predicted background distributions corresponds to the result of the global fit. The signal distribution is normalized to its best fit signal strength. The background histograms are stacked. The "Others" background contribution includes events from diboson and single top quark production, as well as Higgs boson decays to a pair of W bosons. The background uncertainty band accounts for all sources of background uncertainty, systematic as well as statistical, after the global fit. The signal is shown both as a stacked filled histogram and an open overlaid histogram.
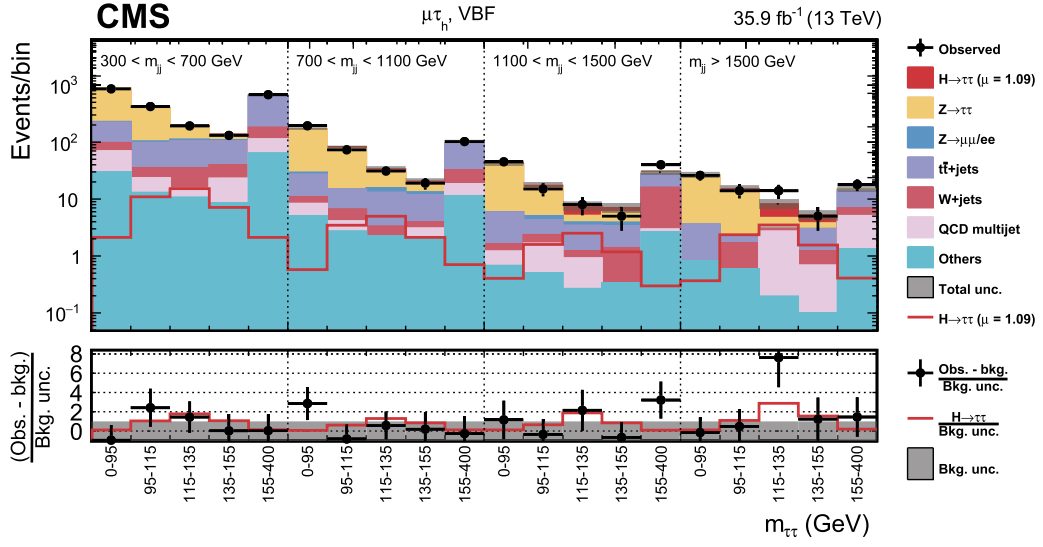
Fig. 7. Observed and predicted 2D distributions in the VBF category of the $\mu\tau_h$ decay channel. The description of the histograms is the same as in Fig. 6.
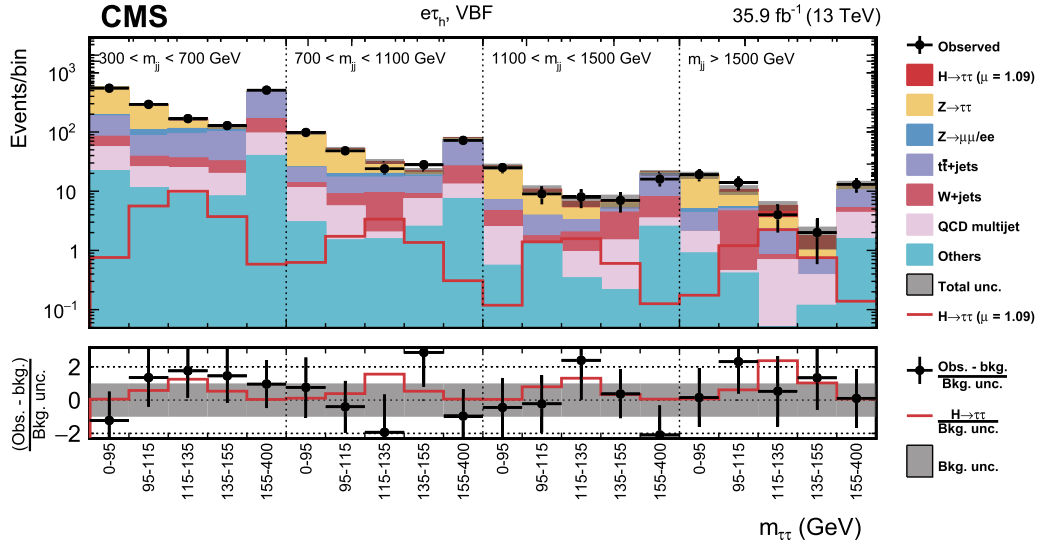

Fig. 8. Observed and predicted 2D distributions in the VBF category of the eτ_h decay channel. The description of the histograms is the same as in Fig. 6.
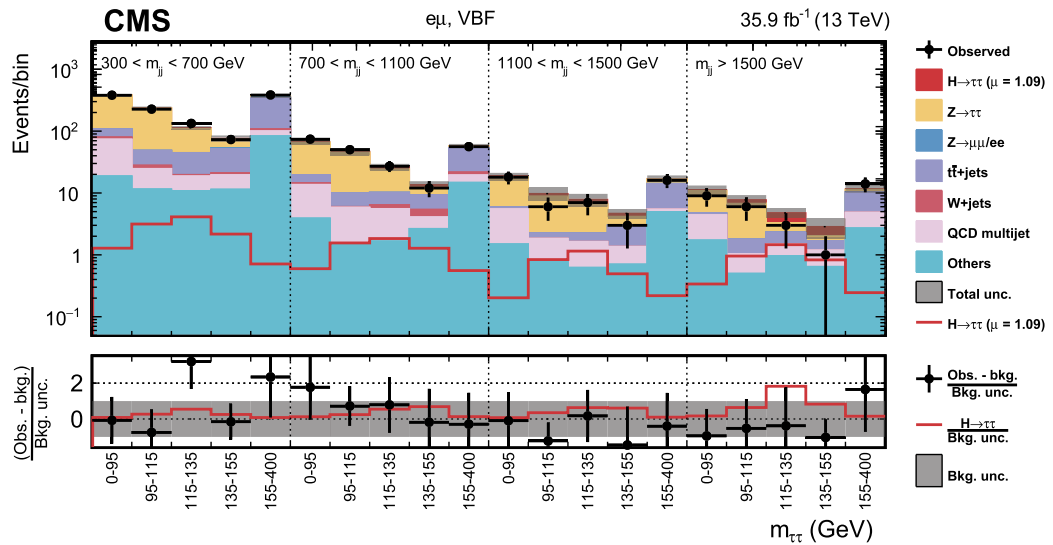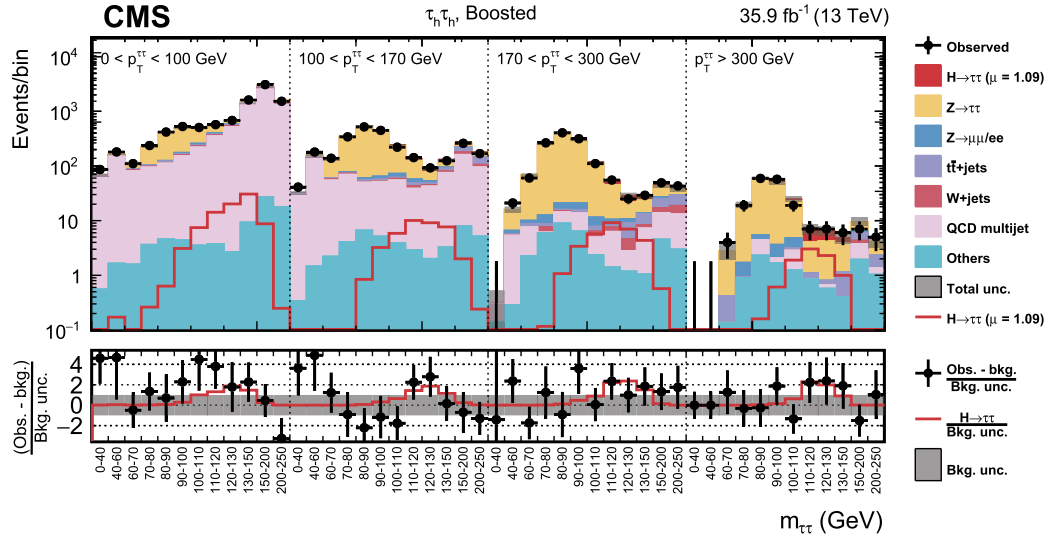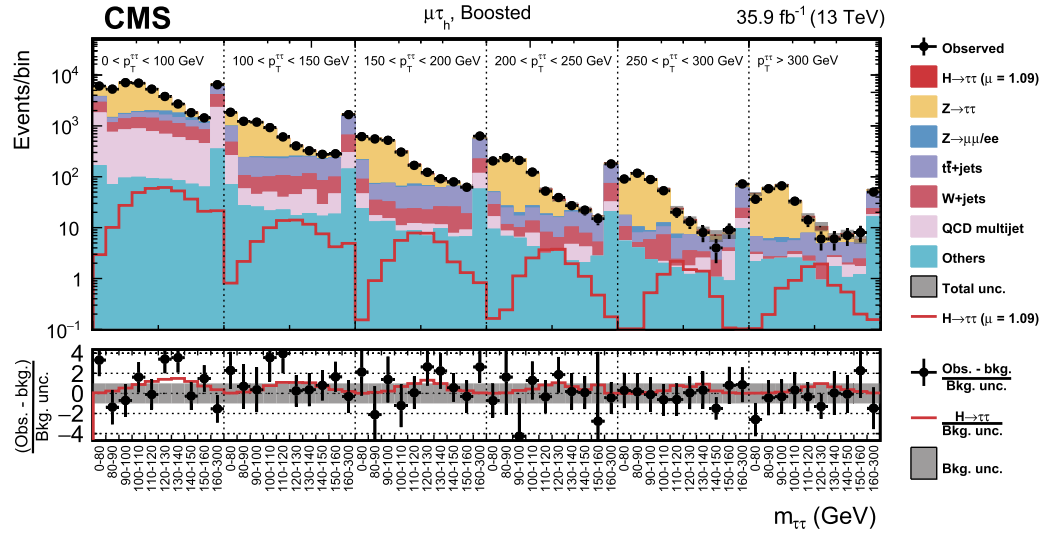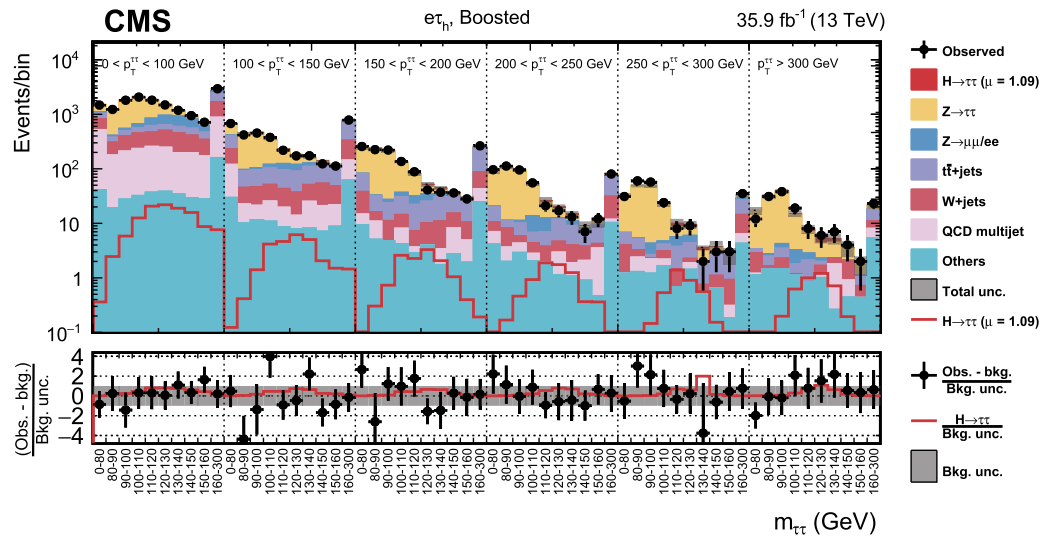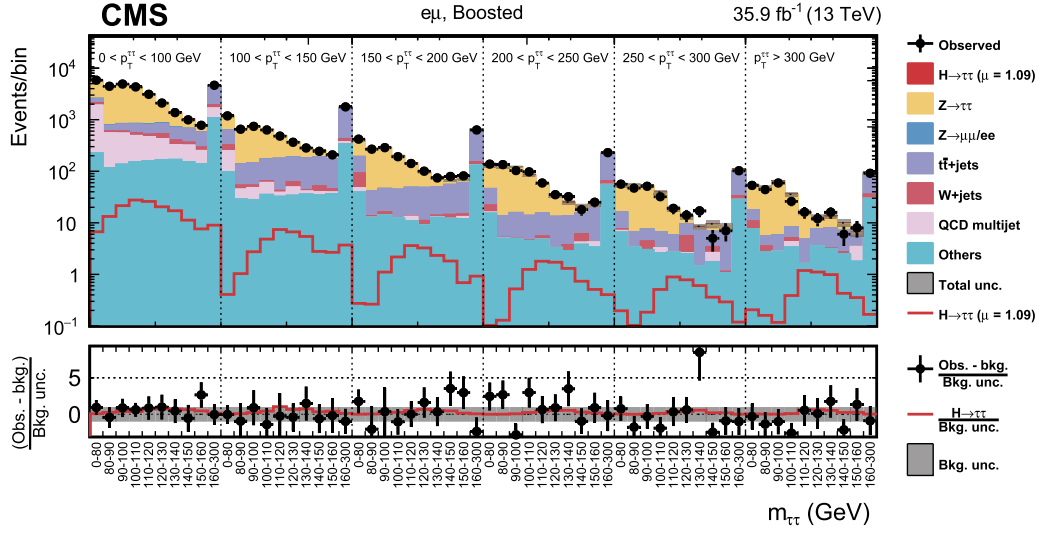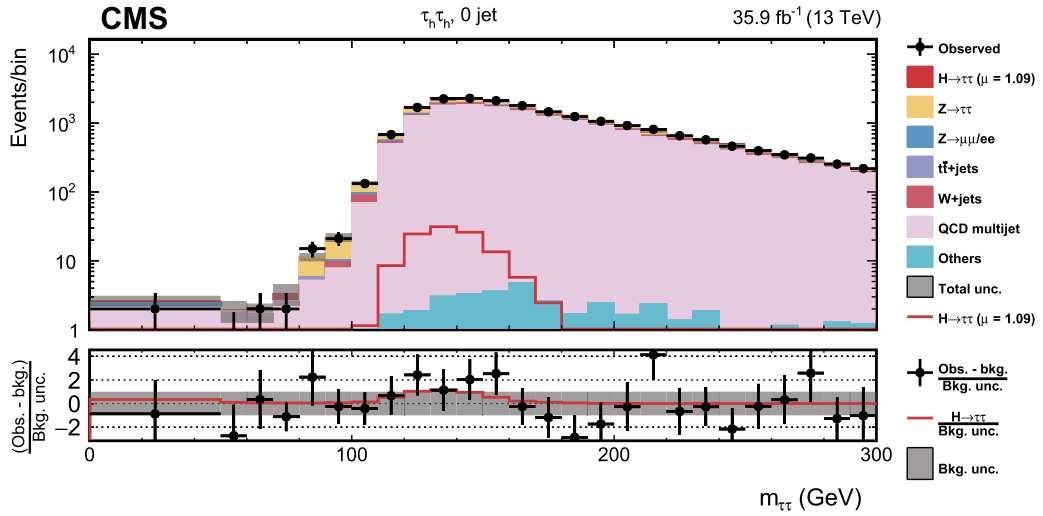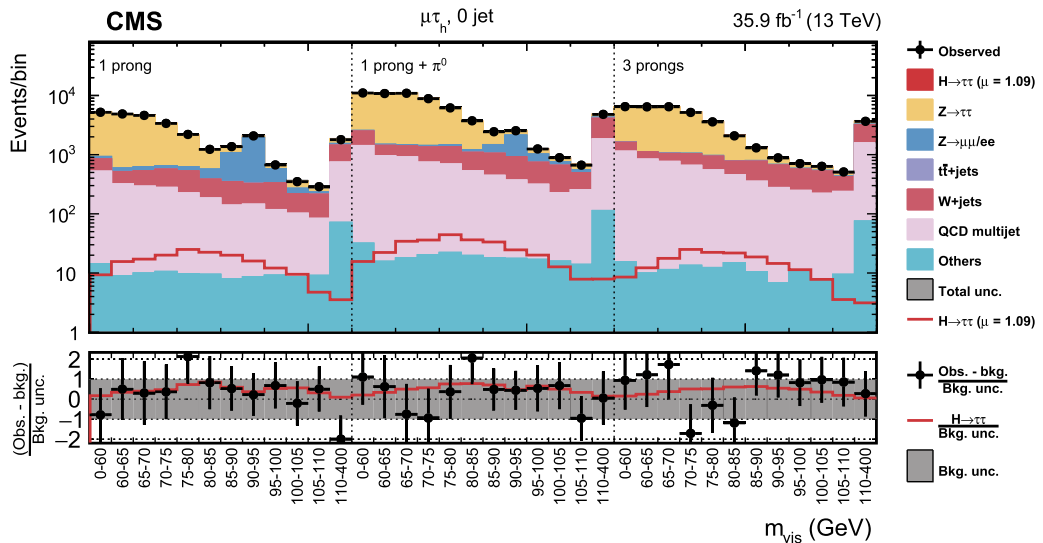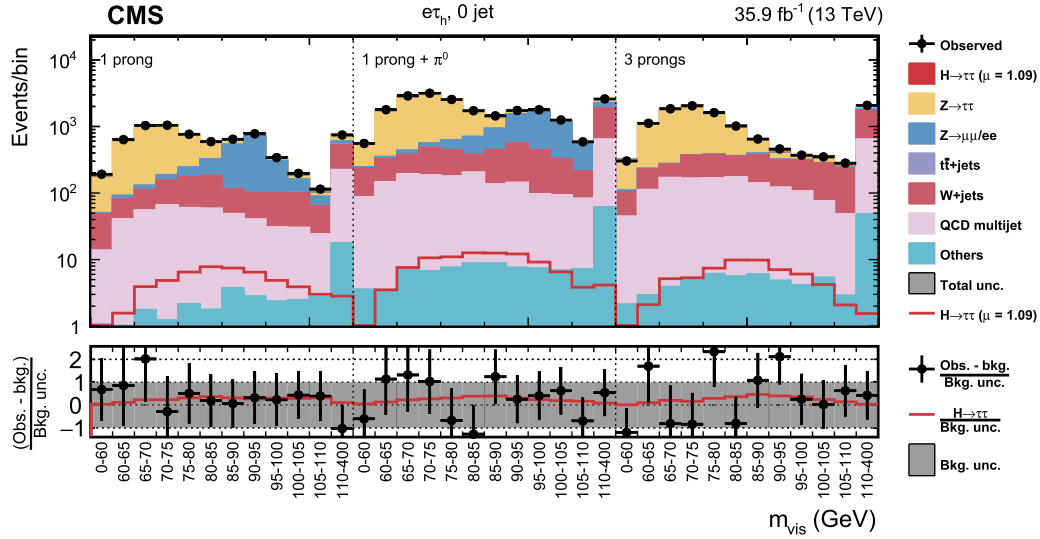

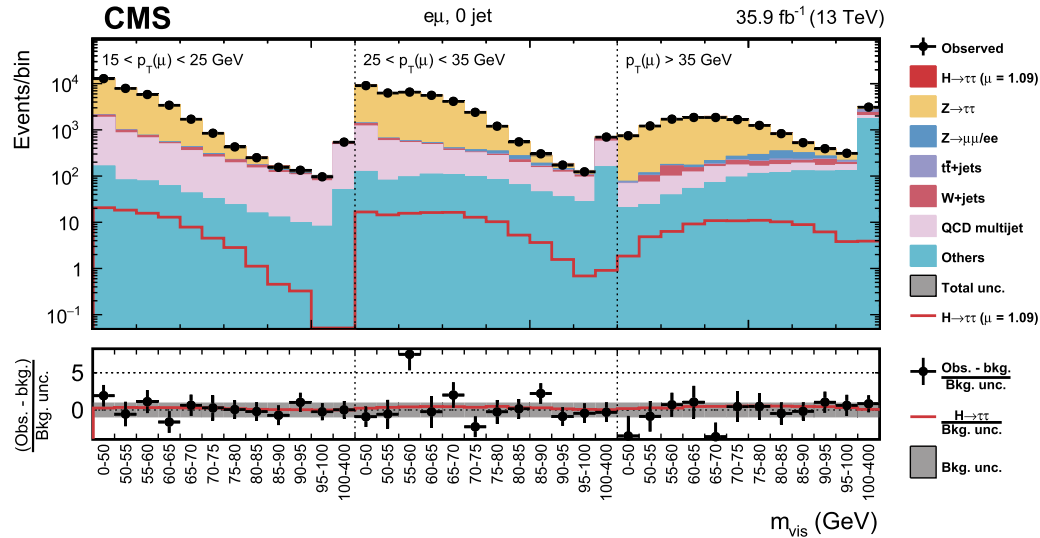
Fig. 9. Observed and predicted 2D distributions in the VBF category of the eμ decay channel. The description of the histograms is the same as in Fig. 6.

Fig. 10. Observed and predicted 2D distributions in the boosted category of the $\tau_h\tau_h$ decay channel. The description of the histograms is the same as in Fig. 6.

Fig. 11. Observed and predicted 2D distributions in the boosted category of the $\mu\tau_h$ decay channel. The description of the histograms is the same as in Fig. 6.

Fig. 12. Observed and predicted 2D distributions in the boosted category of the $e\tau_h$ decay channel. The description of the histograms is the same as in Fig. 6.

Fig. 13. Observed and predicted 2D distributions in the boosted category of the eμ decay channel. The description of the histograms is the same as in Fig. 6.

Fig. 14. Observed and predicted distributions in the 0-jet category of the $\tau_h\tau_h$ decay channel. The description of the histograms is the same as in Fig. 6.

Fig. 15. Observed and predicted 2D distributions in the 0-jet category of the $\mu\tau_h$ decay channel. The description of the histograms is the same as in Fig. 6.

Fig. 16. Observed and predicted 2D distributions in the 0-jet category of the $e\tau_h$ decay channel. The description of the histograms is the same as in Fig. 6.

Fig. 17. Observed and predicted 2D distributions in the 0-jet category of the $e\mu$ decay channel. The description of the histograms is the same as in Fig. 6.

Table 4

Background and signal expectations, together with the number of observed events, for bins in the signal region for which $\log_{10}(S/(S+B)) > -0.9$, where S and B are, respectively, the number of expected signal events for a Higgs boson with a mass $m_H = 125.09$ GeV and of expected background events, in those bins. The background uncertainty accounts for all sources of background uncertainty, systematic as well as statistical, after the global fit. The contribution from "other backgrounds" includes events from diboson and single top quark production. The contribution from Higgs boson decays to a pair of W bosons is zero in these bins.

Process	$e\mu$	$e\tau_h$	$\mu\tau_h$	$\tau_h\tau_h$
$Z \to \tau\tau$	5.8 ± 2.2	21.2 ± 3.3	34.6 ± 4.9	89.1 ± 6.9
$Z \to ee/\mu\mu$	0.0 ± 0.0	2.9 ± 0.2	3.7 ± 0.2	5.0 ± 0.2
$t\bar{t}$ + jets	1.9 ± 0.1	10.4 ± 0.3	22.2 ± 1.8	13.9 ± 0.5
W + jets	0.8 ± 0.02	4.0 ± 0.3	6.6 ± 1.3	7.6 ± 0.8
QCD multijet	2.1 ± 0.3	3.3 ± 2.5	5.0 ± 1.3	35.5 ± 2.1
Other backgrounds	1.4 ± 0.1	5.2 ± 0.2	6.1 ± 0.2	7.3 ± 0.2
ggH, H $\to \tau\tau$	0.6 ± 0.1	5.0 ± 0.6	6.0 ± 0.6	27.4 ± 2.1
VBF H $\to \tau\tau$	2.8 ± 0.3	5.1 ± 0.5	12.55 ± 1.0	17.5 ± 1.0
VH, H $\to \tau\tau$	0.0 ± 0.0	0.3 ± 0.0	0.2 ± 0.0	1.3 ± 0.1
Total backgrounds	12.1 ± 2.2	46.5 ± 4.1	77.7 ± 5.5	156.2 ± 7.3
Total signal	3.4 ± 0.4	10.9 ± 0.8	19.2 ± 1.4	48.3 ± 2.6
Observed	11	54	91	207
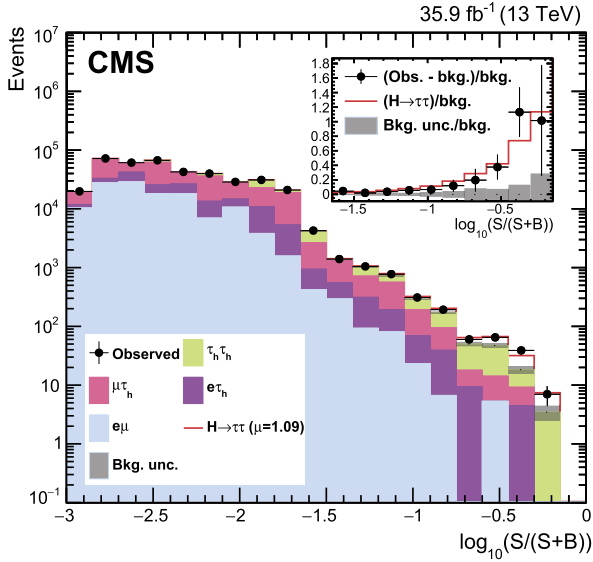
Fig. 18. Distribution of the decimal logarithm of the ratio between the expected signal and the sum of expected signal and expected background in each bin of the mass distributions used to extract the results, in all signal regions. The background contributions are separated by decay channel. The inset shows the corresponding difference between the observed data and expected background distributions divided by the background expectation, as well as the signal expectation divided by the background expectation.

leading to wider bins in the poorly-populated VBF category. The most sensitive category, VBF, is shown first and is followed by the boosted and 0-jet categories. The signal prediction for a Higgs boson with $m_H = 125.09$ GeV is normalized to its best fit cross section times branching fraction. The background distributions are adjusted to the results of the global maximum likelihood fit.

The 2D distributions of the final discriminating variables obtained for each category and each channel in the signal regions, along with the control regions, are combined in a binned likelihood involving the expected and observed numbers of events in each bin. The expected number of signal events is the one predicted for the production of a SM Higgs boson of mass $m_H = 125.09$ GeV decaying into a pair of τ leptons, multiplied by a signal strength modifier μ treated as a free parameter in the fit.

The systematic uncertainties are represented by nuisance parameters that are varied in the fit according to their probability density functions. A log-normal probability density function is assumed for the nuisance parameters affecting the event yields of the various background contributions, whereas systematic uncertainties that affect the shape of the distributions are represented by nuisance parameters whose variation results in a continuous perturbation of the spectrum [69] and which are assumed to have a Gaussian probability density function. Overall, the statistical uncertainty in the observed event yields is the dominant source of uncertainty for all combined results.

Grouping events in the signal region by their decimal logarithm of the ratio of the signal (S) to signal-plus-background ($S + B$) in each bin (Fig. 18), an excess of observed events with respect to the SM background expectation is clearly visible in the most sensitive bins of the analysis. The expected background and signal contributions, as well as the observed number of events, are indicated per process and category in Table 4 for the bins with $\log_{10}(S/(S + B)) > -0.9$. The channel that contributes the most to these bins is $\tau_h\tau_h$.

An excess of observed events relative to the background expectation is also visible in Fig. 19, where every mass distribution for a constant range of the second dimension of the signal distributions
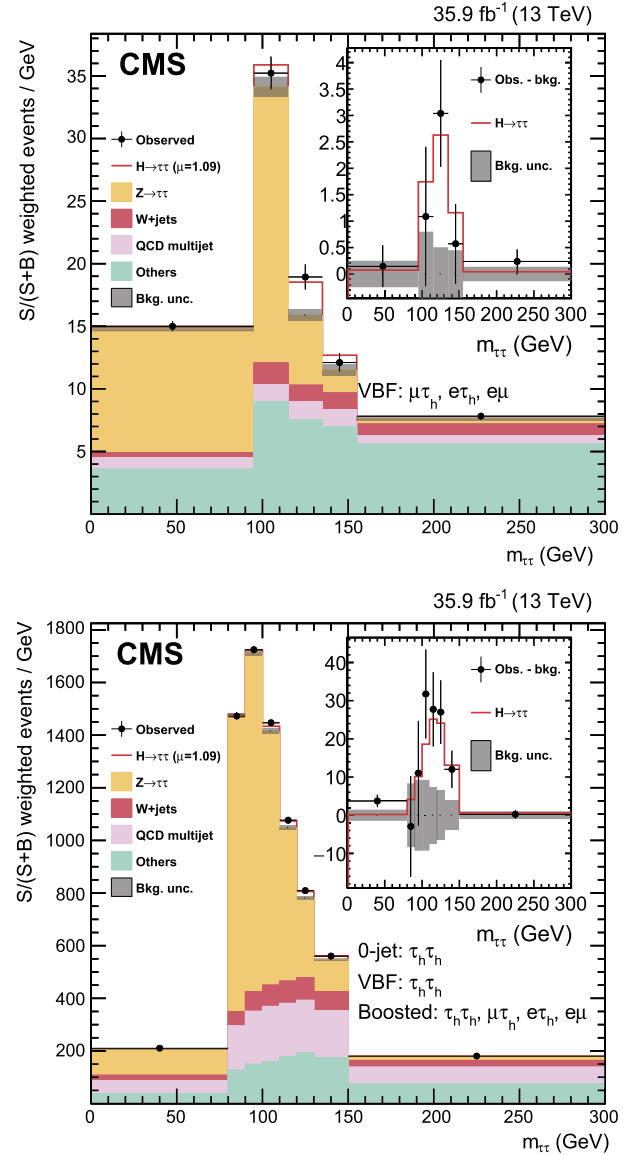
Fig. 19. Combined observed and predicted $m_{\tau\tau}$ distributions. The top panel includes the VBF category of the $\mu\tau_h$, $e\tau_h$ and $e\mu$ channels, and the bottom panel includes all other channels that make use of $m_{\tau\tau}$ instead of m_{vis} for the signal strength fit. The binning reflects the one used in the 2D distributions, and does not allow merging of the two figures. The normalization of the predicted background distributions corresponds to the result of the global fit, while the signal is normalized to its best fit signal strength. The mass distributions for a constant range of the second dimension of the signal distributions are weighted according to $S/(S + B)$, where S and B are computed, respectively, as the signal or background contribution in the mass distribution excluding the first and last bins. The "Others" background contribution includes events from diboson, $t\bar{t}$, and single top quark production, as well as Higgs boson decay to a pair of W bosons and Z bosons decaying to a pair of light leptons. The background uncertainty band accounts for all sources of background uncertainty, systematic as well as statistical, after the global fit. The inset shows the corresponding difference between the observed data and expected background distributions, together with the signal expectation. The signal yield is not affected by the reweighting.

has been summed with a weight of $S/(S + B)$ to increase the contribution of the most sensitive distributions. In this case, S and B are computed, respectively, as the signal or background contribution in the mass distribution excluding the first and last bins, in which the amount of signal is negligible. The signal regions that use m_{vis} instead of $m_{\tau\tau}$, namely the 0-jet category of the $\mu\tau_h$, $e\tau_h$
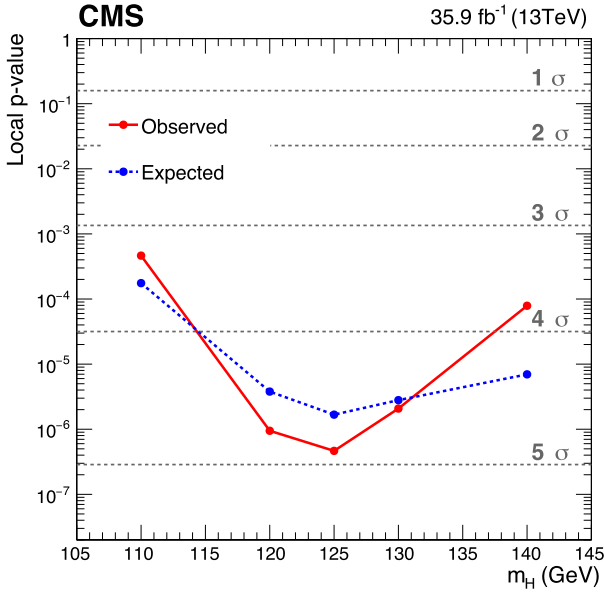
Fig. 20. Local *p*-value and significance as a function of the SM Higgs boson mass hypothesis. The observation (red, solid) is compared to the expectation (blue, dashed) for a Higgs boson with a mass $m_H = 125.09$ GeV. The background includes Higgs boson decays to pairs of W bosons, with $m_H = 125.09$ GeV.

and eμ channels, are not included. The two panes of Fig. 19 group the compatible bins of Figs. 6–17.

The excess in data is quantified by calculating the corresponding local *p*-value using a profile likelihood ratio test statistic [70–73]. As shown in Fig. 20, the observed significance for a SM Higgs boson with $m_H = 125.09$ GeV is 4.9 standard deviations, for an expected significance of 4.7 standard deviations.

The corresponding best fit value for the signal strength μ is $1.09^{+0.27}_{-0.26}$ at $m_H = 125.09$ GeV. The uncertainty in the best fit signal strength can be decomposed into four components: theoretical uncertainties, bin-by-bin statistical uncertainties on the backgrounds, other systematic uncertainties, and the statistical uncertainty. In this format, the best fit signal strength is $\mu = 1.09^{+0.15}_{-0.15}$ (stat)$^{+0.16}_{-0.15}$ (syst)$^{+0.10}_{-0.08}$ (theo)$^{+0.13}_{-0.12}$ (bin-by-bin). The individual best fit signal strengths per channel and per category, using the constraints obtained on the systematic uncertainties through the global fit, are given in Fig. 21; they demonstrate the channel- and category-wise consistency of the observation with the SM Higgs boson hypothesis.

A likelihood scan is performed for $m_H = 125.09$ GeV in the (κ_V, κ_f) parameter space, where κ_V and κ_f quantify, respectively, the ratio between the measured and the SM value for the couplings of the Higgs boson to vector bosons and fermions, with the methods described in Ref. [26]. For this scan only, Higgs boson decays to pairs of W bosons are considered as part of the signal. All nuisance parameters are profiled for each point of the scan. As shown in Fig. 22, the observed likelihood contour is consistent with the SM expectation of κ_V and κ_f equal to unity.

The results are combined with the results of the search for $H \to \tau\tau$ performed with the data collected with the CMS detector at center-of-mass energies of 7 and 8 TeV [14], using a common signal strength for all data taking periods. All uncertainties are considered as fully uncorrelated between the different center-of-mass energies. The combination leads to an observed and an expected significance of 5.9 standard deviations. The corresponding best fit value for the signal strength μ is 0.98 ± 0.18 at $m_H = 125.09$ GeV. This constitutes the most significant direct measurement of the coupling of the Higgs boson to fermions by a single experiment.
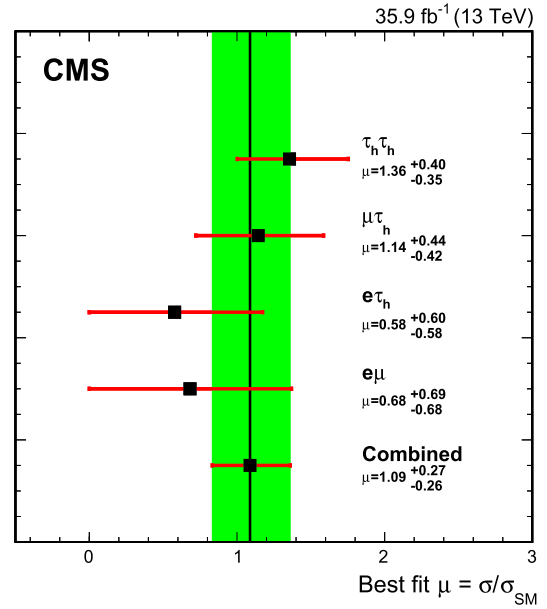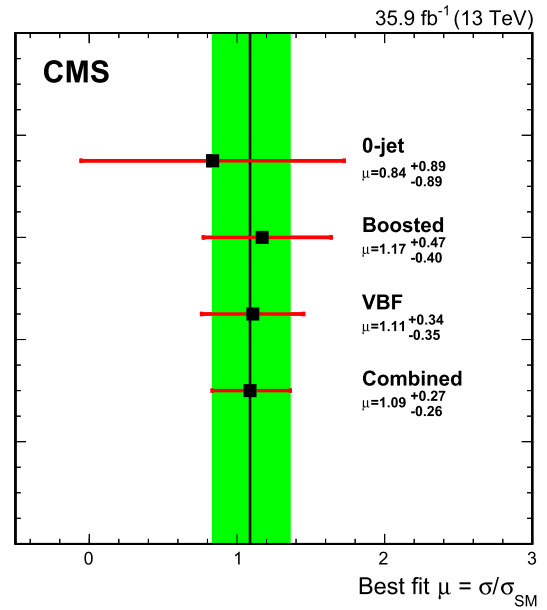
Fig. 21. Best fit signal strength per category (top) and channel (bottom), for $m_H = 125.09$ GeV. The constraints from the global fit are used to extract each of the individual best fit signal strengths. The combined best fit signal strength is $\mu = 1.09^{+0.27}_{-0.26}$.

10. Summary

A measurement of the $H \to \tau\tau$ signal strength, using events recorded in proton–proton collisions by the CMS experiment at the LHC in 2016 at a center-of-mass energy of 13 TeV, has been presented. Event categories are designed to target Higgs boson signal events produced by gluon or vector boson fusion. The results are extracted via maximum likelihood fits in two-dimensional planes, and give an observed significance for Higgs boson decays to τ lepton pairs of 4.9 standard deviations, to be compared with an expected significance of 4.7 standard deviations. The combination with the corresponding measurement performed at center-of-mass energies of 7 and 8 TeV with the CMS detector leads to the first observation by a single experiment of decays of the Higgs boson to pairs of τ leptons, with a significance of 5.9 standard deviations.
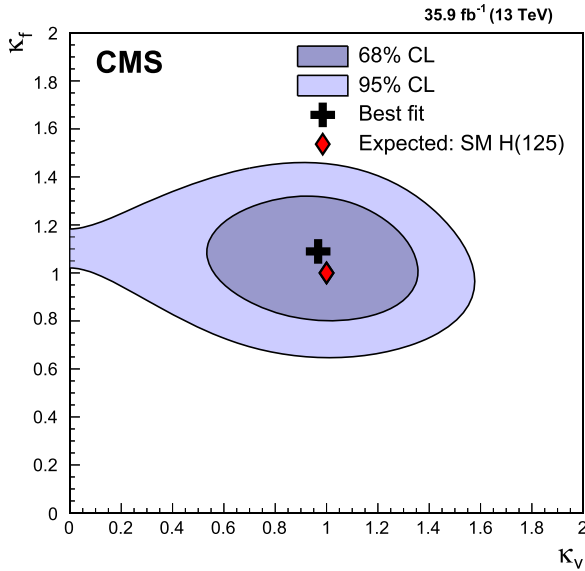
Fig. 22. Scan of the negative log-likelihood difference as a function of κ_V and κ_f, for $m_H = 125.09$ GeV. All nuisance parameters are profiled for each point. For this scan, the $pp \to H \to WW$ contribution is treated as a signal process.

References

[1] S.L. Glashow, Partial-symmetries of weak interactions, Nucl. Phys. 22 (1961) 579, https://doi.org/10.1016/0029-5582(61)90469-2.

[2] S. Weinberg, A model of leptons, Phys. Rev. Lett. 19 (1967) 1264, https://doi.org/10.1103/PhysRevLett.19.1264.

[3] A. Salam, Weak and electromagnetic interactions, in: N. Svartholm (Ed.), Elementary Particle Physics: Relativistic Groups and Analyticity, Almqvist & Wiksell, Stockholm, 1968, p. 367, Proceedings of the Eighth Nobel Symposium.

[4] F. Englert, R. Brout, Broken symmetry and the mass of gauge vector mesons, Phys. Rev. Lett. 13 (1964) 321, https://doi.org/10.1103/PhysRevLett.13.321.

[5] P.W. Higgs, Broken symmetries, massless particles and gauge fields, Phys. Lett. 12 (1964) 132, https://doi.org/10.1016/0031-9163(64)91136-9.

[6] P.W. Higgs, Broken symmetries and the masses of gauge bosons, Phys. Rev. Lett. 13 (1964) 508, https://doi.org/10.1103/PhysRevLett.13.508.

[7] G.S. Guralnik, C.R. Hagen, T.W.B. Kibble, Global conservation laws and massless particles, Phys. Rev. Lett. 13 (1964) 585, https://doi.org/10.1103/PhysRevLett.13.585.

[8] P.W. Higgs, Spontaneous symmetry breakdown without massless bosons, Phys. Rev. 145 (1966) 1156, https://doi.org/10.1103/PhysRev.145.1156.

[9] T.W.B. Kibble, Symmetry breaking in non-abelian gauge theories, Phys. Rev. 155 (1967) 1554, https://doi.org/10.1103/PhysRev.155.1554.

[10] ATLAS Collaboration, Observation of a new particle in the search for the Standard Model Higgs boson with the ATLAS detector at the LHC, Phys. Lett. B 716 (2012) 1, https://doi.org/10.1016/j.physletb.2012.08.020, arXiv:1207.7214.

[11] CMS Collaboration, Observation of a new boson at a mass of 125 GeV with the CMS experiment at the LHC, Phys. Lett. B 716 (2012) 30, https://doi.org/10.1016/j.physletb.2012.08.021, arXiv:1207.7235.

[12] CMS Collaboration, Observation of a new boson with mass near 125 GeV in pp collisions at $\sqrt{s} = 7$ and 8 TeV, J. High Energy Phys. 06 (2013) 081, https://doi.org/10.1007/JHEP06(2013)081, arXiv:1303.4571.

[13] ATLAS Collaboration, Measurements of the Higgs boson production and decay rates and coupling strengths using pp collision data at $\sqrt{s} = 7$ and 8 TeV in the ATLAS experiment, Eur. Phys. J. C 76 (2016) 6, https://doi.org/10.1140/epjc/s10052-015-3769-y, arXiv:1507.04548.

[14] CMS Collaboration, Precise determination of the mass of the Higgs boson and tests of compatibility of its couplings with the standard model predictions using proton collisions at 7 and 8 TeV, Eur. Phys. J. C 75 (2015) 212, https://doi.org/10.1140/epjc/s10052-015-3351-7, arXiv:1412.8662.

[15] CMS Collaboration, Study of the mass and spin-parity of the Higgs boson candidate via its decays to Z boson pairs, Phys. Rev. Lett. 110 (2013) 081803, https://doi.org/10.1103/PhysRevLett.110.081803, arXiv:1212.6639.

[16] ATLAS Collaboration, Evidence for the spin-0 nature of the Higgs boson using ATLAS data, Phys. Lett. B 726 (2013) 120, https://doi.org/10.1016/j.physletb.2013.08.026, arXiv:1307.1432.

[17] CMS Collaboration, Constraints on the spin-parity and anomalous HVV couplings of the Higgs boson in proton collisions at 7 and 8 TeV, Phys. Rev. D 92 (2015) 012004, https://doi.org/10.1103/PhysRevD.92.012004, arXiv:1411.3441.

[18] CMS Collaboration, Measurements of properties of the Higgs boson decaying into the four-lepton final state in pp collisions at $\sqrt{s} = 13$ TeV, J. High Energy Phys. 11 (2018) 047, https://doi.org/10.1007/JHEP11(2017)047, arXiv:1706.09936.

[19] G. Aad, et al., ATLAS and CMS, Combined measurement of the Higgs boson mass in pp collisions at $\sqrt{s} = 7$ and 8 TeV with the ATLAS and CMS experiments, Phys. Rev. Lett. 114 (2015) 191803, https://doi.org/10.1103/PhysRevLett.114.191803, arXiv:1503.07589.

[20] R. Barate, et al., ALEPH, Observation of an excess in the search for the Standard Model Higgs boson at ALEPH, Phys. Lett. B 495 (2000) 1, https://doi.org/10.1016/S0370-2693(00)01269-7, arXiv:hep-ex/0011045.

[21] J. Abdallah, et al., DELPHI, Final results from DELPHI on the searches for SM and MSSM neutral Higgs bosons, Eur. Phys. J. C 32 (2004) 145, https://doi.org/10.1140/epjc/s2003-01394-x, arXiv:hep-ex/0303013.

[22] P. Achard, et al., L3, Standard model Higgs boson with the L3 experiment at LEP, Phys. Lett. B 517 (2001) 319, https://doi.org/10.1016/S0370-2693(01)01010-3, arXiv:hep-ex/0107054.

[23] G. Abbiendi, et al., OPAL, Search for the Standard Model Higgs boson in e^+e^- collisions at $\sqrt{s} = 192$–209 GeV, Phys. Lett. B 499 (2001) 38, https://doi.org/10.1016/S0370-2693(01)00070-3, arXiv:hep-ex/0101014.

[24] T. Aaltonen, et al., CDF, Search for a low-mass Standard Model Higgs boson in the $\tau\tau$ decay channel in $p\bar{p}$ collisions at $\sqrt{s} = 1.96$ TeV, Phys. Rev. Lett. 108 (2012) 181804, https://doi.org/10.1103/PhysRevLett.108.181804, arXiv:1201.4880.

[25] V.M. Abazov, et al., D0, Search for the Standard Model Higgs boson in tau lepton final states, Phys. Lett. B 714 (2012) 237, https://doi.org/10.1016/j.physletb.2012.07.012, arXiv:1203.4443.

[26] CMS Collaboration, Evidence for the 125 GeV Higgs boson decaying to a pair of τ leptons, J. High Energy Phys. 05 (2014) 104, https://doi.org/10.1007/JHEP05(2014)104, arXiv:1401.5041.

[27] ATLAS Collaboration, Evidence for the Higgs-boson Yukawa coupling to tau leptons with the ATLAS detector, J. High Energy Phys. 04 (2015) 117, https://doi.org/10.1007/JHEP04(2015)117, arXiv:1501.04943.

[28] G. Aad, et al., ATLAS, CMS, Measurements of the Higgs boson production and decay rates and constraints on its couplings from a combined ATLAS and CMS analysis of the LHC pp collision data at $\sqrt{s} = 7$ and 8 TeV, J. High Energy Phys. 08 (2016) 045, https://doi.org/10.1007/JHEP08(2016)045, arXiv:1606.02266.

[29] CMS Collaboration, The CMS trigger system, J. Instrum. 12 (2017) P01020, https://doi.org/10.1088/1748-0221/12/01/P01020, arXiv:1609.02366.

[30] CMS Collaboration, The CMS experiment at the CERN LHC, J. Instrum. 3 (2008) S08004, https://doi.org/10.1088/1748-0221/3/08/S08004.

[31] P. Nason, A new method for combining NLO QCD with shower Monte Carlo algorithms, J. High Energy Phys. 11 (2004) 040, https://doi.org/10.1088/1126-6708/2004/11/040, arXiv:hep-ph/0409146.

[32] S. Frixione, P. Nason, C. Oleari, Matching NLO QCD computations with parton shower simulations: the POWHEG method, J. High Energy Phys. 11 (2007) 070, https://doi.org/10.1088/1126-6708/2007/11/070, arXiv:0709.2092.

[33] S. Alioli, P. Nason, C. Oleari, E. Re, A general framework for implementing NLO calculations in shower Monte Carlo programs: the POWHEG BOX, J. High Energy Phys. 06 (2010) 043, https://doi.org/10.1007/JHEP06(2010)043, arXiv:1002.2581.

[34] S. Alioli, K. Hamilton, P. Nason, C. Oleari, E. Re, Jet pair production in POWHEG, J. High Energy Phys. 04 (2011) 081, https://doi.org/10.1007/JHEP04(2011)081, arXiv:1012.3380.

[35] S. Alioli, P. Nason, C. Oleari, E. Re, NLO Higgs boson production via gluon fusion matched with shower in POWHEG, J. High Energy Phys. 04 (2009) 002, https://doi.org/10.1088/1126-6708/2009/04/002, arXiv:0812.0578.

[36] G. Luisoni, P. Nason, C. Oleari, F. Tramontano, $HW^{\pm}/HZ + 0$ and 1 jet at NLO with the POWHEG BOX interfaced to GoSam and their merging within MiNLO, J. High Energy Phys. 10 (2013) 083, https://doi.org/10.1007/JHEP10(2013)083, arXiv:1306.2542.

[37] R.D. Ball, V. Bertone, F. Cerutti, L. Del Debbio, S. Forte, A. Guffanti, J.I. Latorre, J. Rojo, M. Ubiali, Unbiased global determination of parton distributions and their uncertainties at NNLO and at LO, Nucl. Phys. B 855 (2012) 153, https://doi.org/10.1016/j.nuclphysb.2011.09.024, arXiv:1107.2652.

[38] D. de Florian, et al., Handbook of LHC Higgs Cross Sections: 4. Deciphering the Nature of the Higgs Sector, CERN Report CERN-2017-002-M, 2016, https://doi.org/10.23731/CYRM-2017-002, arXiv:1610.07922.

[39] A. Denner, S. Heinemeyer, I. Puljak, D. Rebuzzi, M. Spira, Standard model Higgs-boson branching ratios with uncertainties, Eur. Phys. J. C 71 (2011) 1753, https://doi.org/10.1140/epjc/s10052-011-1753-8, arXiv:1107.5909.

[40] R.D. Ball, et al., NNPDF, Impact of heavy quark masses on parton distributions and LHC phenomenology, Nucl. Phys. B 849 (2011) 296, https://doi.org/10.1016/j.nuclphysb.2011.03.021, arXiv:1101.1300.

[41] J. Alwall, R. Frederix, S. Frixione, V. Hirschi, F. Maltoni, O. Mattelaer, H.S. Shao, T. Stelzer, P. Torrielli, M. Zaro, The automated computation of tree-level and next-to-leading order differential cross sections, and their matching to parton shower simulations, J. High Energy Phys. 07 (2014) 079, https://doi.org/10.1007/JHEP07(2014)079, arXiv:1405.0301.

[42] J. Alwall, S. Höche, F. Krauss, N. Lavesson, L. Lönnblad, F. Maltoni, M.L. Mangano, M. Moretti, C.G. Papadopoulos, F. Piccinini, S. Schumann, M. Treccani, J. Winter, M. Worek, Comparative study of various algorithms for the merging of parton showers and matrix elements in hadronic collisions, Eur. Phys. J. C 53 (2008) 473, https://doi.org/10.1140/epjc/s10052-007-0490-5, arXiv:0706.2569.

[43] R. Frederix, S. Frixione, Merging meets matching in MC@NLO, J. High Energy Phys. 12 (2012) 061, https://doi.org/10.1007/JHEP12(2012)061, arXiv:1209.6215.

[44] T. Sjostrand, S. Ask, J.R. Christiansen, R. Corke, N. Desai, P. Ilten, S. Mrenna, S. Prestel, C.O. Rasmussen, P.Z. Skands, An introduction to PYTHIA 8.2, Comput. Phys. Commun. 191 (2015) 159, https://doi.org/10.1016/j.cpc.2015.01.024, arXiv:1410.3012.

[45] CMS Collaboration, Event generator tunes obtained from underlying event and multiparton scattering measurements, Eur. Phys. J. C 76 (2016) 155, https://doi.org/10.1140/epjc/s10052-016-3988-x, arXiv:1512.00815.

[46] S. Agostinelli, et al., GEANT4, GEANT4 — a simulation toolkit, Nucl. Instrum. Methods A 506 (2003) 250, https://doi.org/10.1016/S0168-9002(03)01368-8.

[47] CMS Collaboration, Particle-flow reconstruction and global event description with the CMS detector, J. Instrum. 12 (2017) P10003, https://doi.org/10.1088/1748-0221/12/10/P10003, arXiv:1706.04965.

[48] M. Cacciari, G.P. Salam, G. Soyez, The anti-k_t jet clustering algorithm, J. High Energy Phys. 04 (2008) 063, https://doi.org/10.1088/1126-6708/2008/04/063, arXiv:0802.1189.

[49] M. Cacciari, G.P. Salam, G. Soyez, FastJet user manual, Eur. Phys. J. C 72 (2012) 1896, https://doi.org/10.1140/epjc/s10052-012-1896-2, arXiv:1111.6097.

[50] CMS Collaboration, Performance of CMS muon reconstruction in pp collision events at $\sqrt{s} = 7$ TeV, J. Instrum. 7 (2012) P10002, https://doi.org/10.1088/1748-0221/7/10/P10002, arXiv:1206.4071.

[51] CMS Collaboration, Performance of electron reconstruction and selection with the CMS detector in proton–proton collisions at $\sqrt{s} = 8$ TeV, J. Instrum. 10 (2015) P06005, https://doi.org/10.1088/1748-0221/10/06/P06005, arXiv:1502.02701.

[52] M. Cacciari, G.P. Salam, Dispelling the N^3 myth for the k_t jet-finder, Phys. Lett. B 641 (2006) 57, https://doi.org/10.1016/j.physletb.2006.08.037, arXiv:hep-ph/0512210.

[53] CMS Collaboration, Determination of jet energy calibration and transverse momentum resolution in CMS, J. Instrum. 6 (2011) 11002, https://doi.org/10.1088/1748-0221/6/11/P11002, arXiv:1107.4277.

[54] CMS Collaboration, Reconstruction and identification of τ lepton decays to hadrons and ν_τ at CMS, J. Instrum. 11 (2016) P01019, https://doi.org/10.1088/1748-0221/11/01/P01019, arXiv:1510.07488.

[55] CMS Collaboration, Performance of Reconstruction and Identification of Tau Leptons in Their Decays to Hadrons and Tau Neutrino in LHC Run-2, CMS Physics Analysis Summary CMS-PAS-TAU-16-002, 2016, https://cds.cern.ch/record/2196972.

[56] H. Voss, A. Höcker, J. Stelzer, F. Tegenfeldt, TMVA, the toolkit for multivariate data analysis with ROOT, in: XI Int. Workshop on Advanced Computing and Analysis Techniques in Physics Research, 2007, http://pos.sissa.it/archive/conferences/050/040/ACAT_040.pdf, arXiv:physics/0703039.

[57] CMS Collaboration, Measurement of the inclusive W and Z production cross sections in pp collisions at $\sqrt{s} = 7$ TeV, J. High Energy Phys. 10 (2011) 132, https://doi.org/10.1007/JHEP10(2011)132, arXiv:1107.4789.

[58] CMS Collaboration, Performance of the CMS missing transverse momentum reconstruction in pp data at $\sqrt{s} = 8$ TeV, J. Instrum. 10 (2015) P02006, https://doi.org/10.1088/1748-0221/10/02/P02006, arXiv:1411.0511.

[59] L. Bianchini, J. Conway, E.K. Friis, C. Veelken, Reconstruction of the Higgs mass in $H \to \tau\tau$ events by dynamical likelihood techniques, J. Phys. Conf. Ser. 513 (2014) 022035, https://doi.org/10.1088/1742-6596/513/2/022035.

[60] CMS Collaboration, Search for neutral MSSM Higgs bosons decaying to a pair of tau leptons in pp collisions, J. High Energy Phys. 10 (2014) 160, https://doi.org/10.1007/JHEP10(2014)160, arXiv:1408.3316.

[61] CMS Collaboration, Performance of Missing Transverse Momentum Reconstruction Algorithms in Proton–Proton Collisions at $\sqrt{s} = 8$ TeV with the CMS Detector, CMS Physics Analysis Summary CMS-PAS-JME-12-002, 2012, http://cdsweb.cern.ch/record/1543527.

[62] CMS Collaboration, Measurement of the WZ production cross section in pp collisions at $\sqrt{s} = 13$ TeV, Phys. Lett. B 766 (2017) 268, https://doi.org/10.1016/j.physletb.2017.01.011, arXiv:1607.06943.

[63] CMS Collaboration, Cross section measurement of t-channel single top quark production in pp collisions at $\sqrt{s} = 13$ TeV, in proofs, Phys. Lett. B (2016), https://doi.org/10.1016/j.physletb.2017.07.047, arXiv:1610.00678.

[64] D. de Florian, G. Ferrera, M. Grazzini, D. Tommasini, Higgs boson production at the LHC: transverse momentum resummation effects in the H $\to \gamma\gamma$, H $\to WW \to l\nu l\nu$ and H $\to ZZ \to 4l$ decay modes, J. High Energy Phys. 06 (2012) 132, https://doi.org/10.1007/JHEP06(2012)132, arXiv:1203.6321.

[65] M. Grazzini, H. Sargsyan, Heavy-quark mass effects in Higgs boson production at the LHC, J. High Energy Phys. 09 (2013) 129, https://doi.org/10.1007/JHEP09(2013)129, arXiv:1306.4581.

[66] J. Bellm, S. Gieseke, D. Grellscheid, A. Papaefstathiou, S. Plätzer, P. Richardson, C. Röhr, T. Schuh, M.H. Seymour, A. Siódmok, A. Wilcock, B. Zimmermann, Herwig++ 2.7 release note, arXiv:1310.6877, 2013.

[67] I.W. Stewart, F.J. Tackmann, Theory uncertainties for Higgs and other searches using jet bins, Phys. Rev. D 85 (2012) 034011, https://doi.org/10.1103/PhysRevD.85.034011, arXiv:1107.2117.

[68] CMS Collaboration, CMS Luminosity Measurements for the 2016 Data Taking Period, CMS Physics Analysis Summary CMS-PAS-LUM-17-001, 2017, https://cds.cern.ch/record/2257069.

[69] J.S. Conway, Incorporating nuisance parameters in likelihoods for multisource spectra, in: Proceedings of PHYSTAT 2011 Workshop on Statistical Issues Related to Discovery Claims in Search Experiments and Unfolding, CERN-2011-006, 2011, p. 115, http://cdsweb.cern.ch/record/1306523.

[70] ATLAS, CMS Collaborations, LHC Higgs Combination Group, Procedure for the LHC Higgs Boson Search Combination in Summer 2011, Technical Report ATL-PHYS-PUB 2011-11, CMS NOTE 2011/005, CERN, 2011, http://cdsweb.cern.ch/record/1379837.

[71] S. Chatrchyan, et al., CMS, Combined results of searches for the Standard Model Higgs boson in pp collisions at $\sqrt{s}$ = 7 TeV, Phys. Lett. B 710 (2012) 26, https://doi.org/10.1016/j.physletb.2012.02.064, arXiv:1202.1488.

[72] T. Junk, Confidence level computation for combining searches with small statistics, Nucl. Instrum. Methods A 434 (1999) 435, https://doi.org/10.1016/S0168-9002(99)00498-2, arXiv:hep-ex/9902006.

[73] A.L. Read, Presentation of search results: the CL_s technique, in: Durham IPPP Workshop: Advanced Statistical Techniques in Particle Physics, Durham, UK, 2002, p. 2693;
J. Phys. G 28 (2002) 2693.

The CMS Collaboration

A.M. Sirunyan, A. Tumasyan

Yerevan Physics Institute, Yerevan, Armenia

W. Adam, F. Ambrogi, E. Asilar, T. Bergauer, J. Brandstetter, E. Brondolin, M. Dragicevic, J. Erö, M. Flechl, M. Friedl, R. Frühwirth [1], V.M. Ghete, J. Grossmann, J. Hrubec, M. Jeitler [1], A. König, N. Krammer, I. Krätschmer, D. Liko, T. Madlener, I. Mikulec, E. Pree, D. Rabady, N. Rad, H. Rohringer, J. Schieck [1], R. Schöfbeck, M. Spanring, D. Spitzbart, W. Waltenberger, J. Wittmann, C.-E. Wulz [1], M. Zarucki

Institut für Hochenergiephysik, Wien, Austria

V. Chekhovsky, V. Mossolov, J. Suarez Gonzalez

Institute for Nuclear Problems, Minsk, Belarus

E.A. De Wolf, D. Di Croce, X. Janssen, J. Lauwers, H. Van Haevermaet, P. Van Mechelen, N. Van Remortel

Universiteit Antwerpen, Antwerpen, Belgium

S. Abu Zeid, F. Blekman, J. D'Hondt, I. De Bruyn, J. De Clercq, K. Deroover, G. Flouris, D. Lontkovskyi, S. Lowette, S. Moortgat, L. Moreels, Q. Python, K. Skovpen, S. Tavernier, W. Van Doninck, P. Van Mulders, I. Van Parijs

Vrije Universiteit Brussel, Brussel, Belgium

D. Beghin, H. Brun, B. Clerbaux, G. De Lentdecker, H. Delannoy, G. Fasanella, L. Favart, R. Goldouzian, A. Grebenyuk, G. Karapostoli, T. Lenzi, J. Luetic, T. Maerschalk, A. Marinov, A. Randle-conde, T. Seva, C. Vander Velde, P. Vanlaer, D. Vannerom, R. Yonamine, F. Zenoni, F. Zhang [2]

Université Libre de Bruxelles, Bruxelles, Belgium

A. Cimmino, T. Cornelis, D. Dobur, A. Fagot, M. Gul, I. Khvastunov, D. Poyraz, C. Roskas, S. Salva, M. Tytgat, W. Verbeke, N. Zaganidis

Ghent University, Ghent, Belgium

H. Bakhshiansohi, O. Bondu, S. Brochet, G. Bruno, C. Caputo, A. Caudron, S. De Visscher, C. Delaere, M. Delcourt, B. Francois, A. Giammanco, A. Jafari, M. Komm, G. Krintiras, V. Lemaitre, A. Magitteri, A. Mertens, M. Musich, K. Piotrzkowski, L. Quertenmont, M. Vidal Marono, S. Wertz

Université Catholique de Louvain, Louvain-la-Neuve, Belgium

N. Beliy

Université de Mons, Mons, Belgium

W.L. Aldá Júnior, F.L. Alves, G.A. Alves, L. Brito, M. Correa Martins Junior, C. Hensel, A. Moraes, M.E. Pol, P. Rebello Teles

Centro Brasileiro de Pesquisas Fisicas, Rio de Janeiro, Brazil

E. Belchior Batista Das Chagas, W. Carvalho, J. Chinellato [3], E. Coelho, A. Custódio, E.M. Da Costa, G.G. Da Silveira [4], D. De Jesus Damiao, S. Fonseca De Souza, L.M. Huertas Guativa, H. Malbouisson,

M. Melo De Almeida, C. Mora Herrera, L. Mundim, H. Nogima, A. Santoro, A. Sznajder, E.J. Tonelli Manganote [3], F. Torres Da Silva De Araujo, A. Vilela Pereira

Universidade do Estado do Rio de Janeiro, Rio de Janeiro, Brazil

S. Ahuja [a], C.A. Bernardes [a], T.R. Fernandez Perez Tomei [a], E.M. Gregores [b], P.G. Mercadante [b], S.F. Novaes [a], Sandra S. Padula [a], D. Romero Abad [b], J.C. Ruiz Vargas [a]

[a] *Universidade Estadual Paulista, São Paulo, Brazil*
[b] *Universidade Federal do ABC, São Paulo, Brazil*

A. Aleksandrov, R. Hadjiiska, P. Iaydjiev, M. Misheva, M. Rodozov, M. Shopova, S. Stoykova, G. Sultanov

Institute for Nuclear Research and Nuclear Energy of Bulgaria Academy of Sciences, Bulgaria

A. Dimitrov, I. Glushkov, L. Litov, B. Pavlov, P. Petkov

University of Sofia, Sofia, Bulgaria

W. Fang [5], X. Gao [5]

Beihang University, Beijing, China

M. Ahmad, J.G. Bian, G.M. Chen, H.S. Chen, M. Chen, Y. Chen, C.H. Jiang, D. Leggat, H. Liao, Z. Liu, F. Romeo, S.M. Shaheen, A. Spiezia, J. Tao, C. Wang, Z. Wang, E. Yazgan, H. Zhang, S. Zhang, J. Zhao

Institute of High Energy Physics, Beijing, China

Y. Ban, G. Chen, Q. Li, S. Liu, Y. Mao, S.J. Qian, D. Wang, Z. Xu

State Key Laboratory of Nuclear Physics and Technology, Peking University, Beijing, China

C. Avila, A. Cabrera, L.F. Chaparro Sierra, C. Florez, C.F. González Hernández, J.D. Ruiz Alvarez

Universidad de Los Andes, Bogota, Colombia

B. Courbon, N. Godinovic, D. Lelas, I. Puljak, P.M. Ribeiro Cipriano, T. Sculac

University of Split, Faculty of Electrical Engineering, Mechanical Engineering and Naval Architecture, Split, Croatia

Z. Antunovic, M. Kovac

University of Split, Faculty of Science, Split, Croatia

V. Brigljevic, D. Ferencek, K. Kadija, B. Mesic, A. Starodumov [6], T. Susa

Institute Rudjer Boskovic, Zagreb, Croatia

M.W. Ather, A. Attikis, G. Mavromanolakis, J. Mousa, C. Nicolaou, F. Ptochos, P.A. Razis, H. Rykaczewski

University of Cyprus, Nicosia, Cyprus

M. Finger [7], M. Finger Jr. [7]

Charles University, Prague, Czech Republic

E. Carrera Jarrin

Universidad San Francisco de Quito, Quito, Ecuador

Y. Assran [8,9], S. Elgammal [9], A. Mahrous [10]

Academy of Scientific Research and Technology of the Arab Republic of Egypt, Egyptian Network of High Energy Physics, Cairo, Egypt

R.K. Dewanjee, M. Kadastik, L. Perrini, M. Raidal, A. Tiko, C. Veelken

National Institute of Chemical Physics and Biophysics, Tallinn, Estonia

P. Eerola, J. Pekkanen, M. Voutilainen

Department of Physics, University of Helsinki, Helsinki, Finland

J. Härkönen, T. Järvinen, V. Karimäki, R. Kinnunen, T. Lampén, K. Lassila-Perini, S. Lehti, T. Lindén, P. Luukka, E. Tuominen, J. Tuominiemi, E. Tuovinen

Helsinki Institute of Physics, Helsinki, Finland

J. Talvitie, T. Tuuva

Lappeenranta University of Technology, Lappeenranta, Finland

M. Besancon, F. Couderc, M. Dejardin, D. Denegri, J.L. Faure, F. Ferri, S. Ganjour, S. Ghosh, A. Givernaud, P. Gras, G. Hamel de Monchenault, P. Jarry, I. Kucher, E. Locci, M. Machet, J. Malcles, G. Negro, J. Rander, A. Rosowsky, M.Ö. Sahin, M. Titov

IRFU, CEA, Université Paris-Saclay, Gif-sur-Yvette, France

A. Abdulsalam, C. Amendola, I. Antropov, S. Baffioni, F. Beaudette, P. Busson, L. Cadamuro, C. Charlot, R. Granier de Cassagnac, M. Jo, S. Lisniak, A. Lobanov, J. Martin Blanco, M. Nguyen, C. Ochando, G. Ortona, P. Paganini, P. Pigard, R. Salerno, J.B. Sauvan, Y. Sirois, A.G. Stahl Leiton, T. Strebler, Y. Yilmaz, A. Zabi, A. Zghiche

Laboratoire Leprince-Ringuet, Ecole polytechnique, CNRS/IN2P3, Université Paris-Saclay, Palaiseau, France

J.-L. Agram [11], J. Andrea, D. Bloch, J.-M. Brom, M. Buttignol, E.C. Chabert, N. Chanon, C. Collard, E. Conte [11], X. Coubez, J.-C. Fontaine [11], D. Gelé, U. Goerlach, M. Jansová, A.-C. Le Bihan, N. Tonon, P. Van Hove

Université de Strasbourg, CNRS, IPHC UMR 7178, F-67000 Strasbourg, France

S. Gadrat

Centre de Calcul de l'Institut National de Physique Nucléaire et de Physique des Particules, CNRS/IN2P3, Villeurbanne, France

S. Beauceron, C. Bernet, G. Boudoul, R. Chierici, D. Contardo, P. Depasse, H. El Mamouni, J. Fay, L. Finco, S. Gascon, M. Gouzevitch, G. Grenier, B. Ille, F. Lagarde, I.B. Laktineh, M. Lethuillier, L. Mirabito, A.L. Pequegnot, S. Perries, A. Popov [12], V. Sordini, M. Vander Donckt, S. Viret

Université de Lyon, Université Claude Bernard Lyon 1, CNRS-IN2P3, Institut de Physique Nucléaire de Lyon, Villeurbanne, France

A. Khvedelidze [7]

Georgian Technical University, Tbilisi, Georgia

Z. Tsamalaidze [7]

Tbilisi State University, Tbilisi, Georgia

C. Autermann, L. Feld, M.K. Kiesel, K. Klein, M. Lipinski, M. Preuten, C. Schomakers, J. Schulz, T. Verlage, V. Zhukov [12]

RWTH Aachen University, I. Physikalisches Institut, Aachen, Germany

A. Albert, E. Dietz-Laursonn, D. Duchardt, M. Endres, M. Erdmann, S. Erdweg, T. Esch, R. Fischer, A. Güth, M. Hamer, T. Hebbeker, C. Heidemann, K. Hoepfner, S. Knutzen, M. Merschmeyer, A. Meyer, P. Millet, S. Mukherjee, T. Pook, M. Radziej, H. Reithler, M. Rieger, F. Scheuch, D. Teyssier, S. Thüer

RWTH Aachen University, III. Physikalisches Institut A, Aachen, Germany

G. Flügge, B. Kargoll, T. Kress, A. Künsken, J. Lingemann, T. Müller, A. Nehrkorn, A. Nowack, C. Pistone, O. Pooth, A. Stahl [13]

RWTH Aachen University, III. Physikalisches Institut B, Aachen, Germany

M. Aldaya Martin, T. Arndt, C. Asawatangtrakuldee, K. Beernaert, O. Behnke, U. Behrens, A. Bermúdez Martínez, A.A. Bin Anuar, K. Borras [14], V. Botta, A. Campbell, P. Connor, C. Contreras-Campana, F. Costanza, C. Diez Pardos, G. Eckerlin, D. Eckstein, T. Eichhorn, E. Eren, E. Gallo [15], J. Garay Garcia, A. Geiser, A. Gizhko, J.M. Grados Luyando, A. Grohsjean, P. Gunnellini, M. Guthoff, A. Harb, J. Hauk, M. Hempel [16], H. Jung, A. Kalogeropoulos, M. Kasemann, J. Keaveney, C. Kleinwort, I. Korol, D. Krücker, W. Lange, A. Lelek, T. Lenz, J. Leonard, K. Lipka, W. Lohmann [16], R. Mankel, I.-A. Melzer-Pellmann, A.B. Meyer, G. Mittag, J. Mnich, A. Mussgiller, E. Ntomari, D. Pitzl, A. Raspereza, B. Roland, M. Savitskyi, P. Saxena, R. Shevchenko, S. Spannagel, N. Stefaniuk, G.P. Van Onsem, R. Walsh, Y. Wen, K. Wichmann, C. Wissing, O. Zenaiev

Deutsches Elektronen-Synchrotron, Hamburg, Germany

S. Bein, V. Blobel, M. Centis Vignali, T. Dreyer, E. Garutti, D. Gonzalez, J. Haller, A. Hinzmann, M. Hoffmann, A. Karavdina, R. Klanner, R. Kogler, N. Kovalchuk, S. Kurz, T. Lapsien, I. Marchesini, D. Marconi, M. Meyer, M. Niedziela, D. Nowatschin, F. Pantaleo [13], T. Peiffer, A. Perieanu, C. Scharf, P. Schleper, A. Schmidt, S. Schumann, J. Schwandt, J. Sonneveld, H. Stadie, G. Steinbrück, F.M. Stober, M. Stöver, H. Tholen, D. Troendle, E. Usai, L. Vanelderen, A. Vanhoefer, B. Vormwald

University of Hamburg, Hamburg, Germany

M. Akbiyik, C. Barth, S. Baur, E. Butz, R. Caspart, T. Chwalek, F. Colombo, W. De Boer, A. Dierlamm, B. Freund, R. Friese, M. Giffels, D. Haitz, F. Hartmann [13], S.M. Heindl, U. Husemann, F. Kassel [13], S. Kudella, H. Mildner, M.U. Mozer, Th. Müller, M. Plagge, G. Quast, K. Rabbertz, M. Schröder, I. Shvetsov, G. Sieber, H.J. Simonis, R. Ulrich, S. Wayand, M. Weber, T. Weiler, S. Williamson, C. Wöhrmann, R. Wolf

Institut für Experimentelle Kernphysik, Karlsruhe, Germany

G. Anagnostou, G. Daskalakis, T. Geralis, V.A. Giakoumopoulou, A. Kyriakis, D. Loukas, I. Topsis-Giotis

Institute of Nuclear and Particle Physics (INPP), NCSR Demokritos, Aghia Paraskevi, Greece

G. Karathanasis, S. Kesisoglou, A. Panagiotou, N. Saoulidou

National and Kapodistrian University of Athens, Athens, Greece

K. Kousouris

National Technical University of Athens, Athens, Greece

I. Evangelou, C. Foudas, P. Kokkas, S. Mallios, N. Manthos, I. Papadopoulos, E. Paradas, J. Strologas, F.A. Triantis

University of Ioánnina, Ioánnina, Greece

M. Csanad, N. Filipovic, G. Pasztor, G.I. Veres [17]

MTA-ELTE Lendület CMS Particle and Nuclear Physics Group, Eötvös Loránd University, Budapest, Hungary

G. Bencze, C. Hajdu, D. Horvath [18], Á. Hunyadi, F. Sikler, V. Veszpremi, A.J. Zsigmond

Wigner Research Centre for Physics, Budapest, Hungary

N. Beni, S. Czellar, J. Karancsi [19], A. Makovec, J. Molnar, Z. Szillasi

Institute of Nuclear Research ATOMKI, Debrecen, Hungary

M. Bartók [17], P. Raics, Z.L. Trocsanyi, B. Ujvari

Institute of Physics, University of Debrecen, Debrecen, Hungary

S. Choudhury, J.R. Komaragiri

Indian Institute of Science (IISc), Bangalore, India

S. Bahinipati [20], S. Bhowmik, P. Mal, K. Mandal, A. Nayak [21], D.K. Sahoo [20], N. Sahoo, S.K. Swain

National Institute of Science Education and Research, Bhubaneswar, India

S. Bansal, S.B. Beri, V. Bhatnagar, R. Chawla, N. Dhingra, A.K. Kalsi, A. Kaur, M. Kaur, R. Kumar, P. Kumari, A. Mehta, J.B. Singh, G. Walia

Panjab University, Chandigarh, India

Ashok Kumar, Aashaq Shah, A. Bhardwaj, S. Chauhan, B.C. Choudhary, R.B. Garg, S. Keshri, A. Kumar, S. Malhotra, M. Naimuddin, K. Ranjan, R. Sharma

University of Delhi, Delhi, India

R. Bhardwaj, R. Bhattacharya, S. Bhattacharya, U. Bhawandeep, S. Dey, S. Dutt, S. Dutta, S. Ghosh, N. Majumdar, A. Modak, K. Mondal, S. Mukhopadhyay, S. Nandan, A. Purohit, A. Roy, D. Roy, S. Roy Chowdhury, S. Sarkar, M. Sharan, S. Thakur

Saha Institute of Nuclear Physics, HBNI, Kolkata, India

P.K. Behera

Indian Institute of Technology Madras, Madras, India

R. Chudasama, D. Dutta, V. Jha, V. Kumar, A.K. Mohanty [13], P.K. Netrakanti, L.M. Pant, P. Shukla, A. Topkar

Bhabha Atomic Research Centre, Mumbai, India

T. Aziz, S. Dugad, B. Mahakud, S. Mitra, G.B. Mohanty, N. Sur, B. Sutar

Tata Institute of Fundamental Research-A, Mumbai, India

S. Banerjee, S. Bhattacharya, S. Chatterjee, P. Das, M. Guchait, Sa. Jain, S. Kumar, M. Maity [22], G. Majumder, K. Mazumdar, T. Sarkar [22], N. Wickramage [23]

Tata Institute of Fundamental Research-B, Mumbai, India

S. Chauhan, S. Dube, V. Hegde, A. Kapoor, K. Kothekar, S. Pandey, A. Rane, S. Sharma

Indian Institute of Science Education and Research (IISER), Pune, India

S. Chenarani [24], E. Eskandari Tadavani, S.M. Etesami [24], M. Khakzad, M. Mohammadi Najafabadi, M. Naseri, S. Paktinat Mehdiabadi [25], F. Rezaei Hosseinabadi, B. Safarzadeh [26], M. Zeinali

Institute for Research in Fundamental Sciences (IPM), Tehran, Iran

M. Felcini, M. Grunewald

University College Dublin, Dublin, Ireland

M. Abbrescia [a,b], C. Calabria [a,b], A. Colaleo [a], D. Creanza [a,c], L. Cristella [a,b], N. De Filippis [a,c], M. De Palma [a,b], F. Errico [a,b], L. Fiore [a], G. Iaselli [a,c], S. Lezki [a,b], G. Maggi [a,c], M. Maggi [a], G. Miniello [a,b], S. My [a,b], S. Nuzzo [a,b], A. Pompili [a,b], G. Pugliese [a,c], R. Radogna [a], A. Ranieri [a], G. Selvaggi [a,b], A. Sharma [a], L. Silvestris [a,13], R. Venditti [a], P. Verwilligen [a]

[a] *INFN Sezione di Bari, Bari, Italy*
[b] *Università di Bari, Bari, Italy*
[c] *Politecnico di Bari, Bari, Italy*

G. Abbiendi [a], C. Battilana [a,b], D. Bonacorsi [a,b], S. Braibant-Giacomelli [a,b], R. Campanini [a,b], P. Capiluppi [a,b], A. Castro [a,b], F.R. Cavallo [a], S.S. Chhibra [a], G. Codispoti [a,b], M. Cuffiani [a,b], G.M. Dallavalle [a], F. Fabbri [a], A. Fanfani [a,b], D. Fasanella [a,b], P. Giacomelli [a], C. Grandi [a], L. Guiducci [a,b], S. Marcellini [a], G. Masetti [a], A. Montanari [a], F.L. Navarria [a,b], A. Perrotta [a], A.M. Rossi [a,b], T. Rovelli [a,b], G.P. Siroli [a,b], N. Tosi [a]

[a] *INFN Sezione di Bologna, Bologna, Italy*
[b] *Università di Bologna, Bologna, Italy*

S. Albergo [a,b], S. Costa [a,b], A. Di Mattia [a], F. Giordano [a,b], R. Potenza [a,b], A. Tricomi [a,b], C. Tuve [a,b]

[a] *INFN Sezione di Catania, Catania, Italy*
[b] *Università di Catania, Catania, Italy*

G. Barbagli [a], K. Chatterjee [a,b], V. Ciulli [a,b], C. Civinini [a], R. D'Alessandro [a,b], E. Focardi [a,b], P. Lenzi [a,b], M. Meschini [a], S. Paoletti [a], L. Russo [a,27], G. Sguazzoni [a], D. Strom [a], L. Viliani [a,b,13]

[a] *INFN Sezione di Firenze, Firenze, Italy*
[b] *Università di Firenze, Firenze, Italy*

L. Benussi, S. Bianco, F. Fabbri, D. Piccolo, F. Primavera [13]

INFN Laboratori Nazionali di Frascati, Frascati, Italy

V. Calvelli [a,b], F. Ferro [a], E. Robutti [a], S. Tosi [a,b]

[a] *INFN Sezione di Genova, Genova, Italy*
[b] *Università di Genova, Genova, Italy*

A. Benaglia [a], L. Brianza [a,b], F. Brivio [a,b], V. Ciriolo [a,b], M.E. Dinardo [a,b], S. Fiorendi [a,b], S. Gennai [a], A. Ghezzi [a,b], P. Govoni [a,b], M. Malberti [a,b], S. Malvezzi [a], R.A. Manzoni [a,b], D. Menasce [a], L. Moroni [a], M. Paganoni [a,b], K. Pauwels [a,b], D. Pedrini [a], S. Pigazzini [a,b,28], S. Ragazzi [a,b], N. Redaelli [a], T. Tabarelli de Fatis [a,b]

[a] *INFN Sezione di Milano-Bicocca, Milano, Italy*
[b] *Università di Milano-Bicocca, Milano, Italy*

S. Buontempo [a], N. Cavallo [a,c], S. Di Guida [a,d,13], F. Fabozzi [a,c], F. Fienga [a,b], A.O.M. Iorio [a,b], W.A. Khan [a], L. Lista [a], S. Meola [a,d,13], P. Paolucci [a,13], C. Sciacca [a,b], F. Thyssen [a]

[a] *INFN Sezione di Napoli, Napoli, Italy*
[b] *Università di Napoli 'Federico II', Napoli, Italy*
[c] *Università della Basilicata, Potenza, Italy*
[d] *Università G. Marconi, Roma, Italy*

P. Azzi [a], N. Bacchetta [a], L. Benato [a,b], D. Bisello [a,b], A. Boletti [a,b], A. Bragagnolo, R. Carlin [a,b], A. Carvalho Antunes De Oliveira [a,b], P. Checchia [a], M. Dall'Osso [a,b], P. De Castro Manzano [a], T. Dorigo [a], U. Dosselli [a], F. Gasparini [a,b], U. Gasparini [a,b], S. Lacaprara [a], P. Lujan, M. Margoni [a,b], A.T. Meneguzzo [a,b], N. Pozzobon [a,b], P. Ronchese [a,b], R. Rossin [a,b], F. Simonetto [a,b], E. Torassa [a], S. Ventura [a], M. Zanetti [a,b], P. Zotto [a,b]

[a] *INFN Sezione di Padova, Padova, Italy*
[b] *Università di Padova, Padova, Italy*
[c] *Università di Trento, Trento, Italy*

A. Braghieri [a], A. Magnani [a], P. Montagna [a,b], S.P. Ratti [a,b], V. Re [a], M. Ressegotti [a,b], C. Riccardi [a,b], P. Salvini [a], I. Vai [a,b], P. Vitulo [a,b]

[a] *INFN Sezione di Pavia, Pavia, Italy*
[b] *Università di Pavia, Pavia, Italy*

L. Alunni Solestizi [a,b], M. Biasini [a,b], G.M. Bilei [a], C. Cecchi [a,b], D. Ciangottini [a,b], L. Fanò [a,b], P. Lariccia [a,b], R. Leonardi [a,b], E. Manoni [a], G. Mantovani [a,b], V. Mariani [a,b], M. Menichelli [a], A. Rossi [a,b], A. Santocchia [a,b], D. Spiga [a]

[a] *INFN Sezione di Perugia, Perugia, Italy*

[b] *Università di Perugia, Perugia, Italy*

K. Androsov [a], P. Azzurri [a,13], G. Bagliesi [a], T. Boccali [a], L. Borrello, R. Castaldi [a], M.A. Ciocci [a,b], R. Dell'Orso [a], G. Fedi [a], L. Giannini [a,c], A. Giassi [a], M.T. Grippo [a,27], F. Ligabue [a,c], T. Lomtadze [a], E. Manca [a,c], G. Mandorli [a,c], L. Martini [a,b], A. Messineo [a,b], F. Palla [a], A. Rizzi [a,b], A. Savoy-Navarro [a,29], P. Spagnolo [a], R. Tenchini [a], G. Tonelli [a,b], A. Venturi [a], P.G. Verdini [a]

[a] *INFN Sezione di Pisa, Pisa, Italy*
[b] *Università di Pisa, Pisa, Italy*
[c] *Scuola Normale Superiore di Pisa, Pisa, Italy*

L. Barone [a,b], F. Cavallari [a], M. Cipriani [a,b], N. Daci [a], D. Del Re [a,b,13], E. Di Marco [a,b], M. Diemoz [a], S. Gelli [a,b], E. Longo [a,b], F. Margaroli [a,b], B. Marzocchi [a,b], P. Meridiani [a], G. Organtini [a,b], R. Paramatti [a,b], F. Preiato [a,b], S. Rahatlou [a,b], C. Rovelli [a], F. Santanastasio [a,b]

[a] *INFN Sezione di Roma, Rome, Italy*
[b] *Sapienza Università di Roma, Rome, Italy*

N. Amapane [a,b], R. Arcidiacono [a,c], S. Argiro [a,b], M. Arneodo [a,c], N. Bartosik [a], R. Bellan [a,b], C. Biino [a], N. Cartiglia [a], F. Cenna [a,b], M. Costa [a,b], R. Covarelli [a,b], A. Degano [a,b], N. Demaria [a], B. Kiani [a,b], C. Mariotti [a], S. Maselli [a], E. Migliore [a,b], V. Monaco [a,b], E. Monteil [a,b], M. Monteno [a], M.M. Obertino [a,b], L. Pacher [a,b], N. Pastrone [a], M. Pelliccioni [a], G.L. Pinna Angioni [a,b], F. Ravera [a,b], A. Romero [a,b], M. Ruspa [a,c], R. Sacchi [a,b], K. Shchelina [a,b], V. Sola [a], A. Solano [a,b], A. Staiano [a], P. Traczyk [a,b]

[a] *INFN Sezione di Torino, Torino, Italy*
[b] *Università di Torino, Torino, Italy*
[c] *Università del Piemonte Orientale, Novara, Italy*

S. Belforte [a], M. Casarsa [a], F. Cossutti [a], G. Della Ricca [a,b], A. Zanetti [a]

[a] *INFN Sezione di Trieste, Trieste, Italy*
[b] *Università di Trieste, Trieste, Italy*

D.H. Kim, G.N. Kim, M.S. Kim, J. Lee, S. Lee, S.W. Lee, C.S. Moon, Y.D. Oh, S. Sekmen, D.C. Son, Y.C. Yang

Kyungpook National University, Daegu, Republic of Korea

A. Lee

Chonbuk National University, Jeonju, Republic of Korea

H. Kim, D.H. Moon, G. Oh

Chonnam National University, Institute for Universe and Elementary Particles, Kwangju, Republic of Korea

J.A. Brochero Cifuentes, J. Goh, T.J. Kim

Hanyang University, Seoul, Republic of Korea

S. Cho, S. Choi, Y. Go, D. Gyun, S. Ha, B. Hong, Y. Jo, Y. Kim, K. Lee, K.S. Lee, S. Lee, J. Lim, S.K. Park, Y. Roh

Korea University, Seoul, Republic of Korea

J. Almond, J. Kim, J.S. Kim, H. Lee, K. Lee, K. Nam, S.B. Oh, B.C. Radburn-Smith, S.h. Seo, U.K. Yang, H.D. Yoo, G.B. Yu

Seoul National University, Seoul, Republic of Korea

M. Choi, H. Kim, J.H. Kim, J.S.H. Lee, I.C. Park

University of Seoul, Seoul, Republic of Korea

Y. Choi, C. Hwang, J. Lee, I. Yu

Sungkyunkwan University, Suwon, Republic of Korea

V. Dudenas, A. Juodagalvis, J. Vaitkus

Vilnius University, Vilnius, Lithuania

I. Ahmed, Z.A. Ibrahim, M.A.B. Md Ali [30], F. Mohamad Idris [31], W.A.T. Wan Abdullah, M.N. Yusli, Z. Zolkapli

National Centre for Particle Physics, Universiti Malaya, Kuala Lumpur, Malaysia

R. Reyes-Almanza, G. Ramirez-Sanchez, M.C. Duran-Osuna, H. Castilla-Valdez, E. De La Cruz-Burelo, I. Heredia-De La Cruz [32], R.I. Rabadan-Trejo, R. Lopez-Fernandez, J. Mejia Guisao, A. Sanchez-Hernandez

Centro de Investigacion y de Estudios Avanzados del IPN, Mexico City, Mexico

S. Carrillo Moreno, C. Oropeza Barrera, F. Vazquez Valencia

Universidad Iberoamericana, Mexico City, Mexico

I. Pedraza, H.A. Salazar Ibarguen, C. Uribe Estrada

Benemerita Universidad Autonoma de Puebla, Puebla, Mexico

A. Morelos Pineda

Universidad Autónoma de San Luis Potosí, San Luis Potosí, Mexico

D. Krofcheck

University of Auckland, Auckland, New Zealand

P.H. Butler

University of Canterbury, Christchurch, New Zealand

A. Ahmad, M. Ahmad, Q. Hassan, H.R. Hoorani, A. Saddique, M.A. Shah, M. Shoaib, M. Waqas

National Centre for Physics, Quaid-I-Azam University, Islamabad, Pakistan

H. Bialkowska, M. Bluj, B. Boimska, T. Frueboes, M. Górski, M. Kazana, K. Nawrocki, M. Szleper, P. Zalewski

National Centre for Nuclear Research, Swierk, Poland

K. Bunkowski, A. Byszuk [33], K. Doroba, A. Kalinowski, M. Konecki, J. Krolikowski, M. Misiura, M. Olszewski, A. Pyskir, M. Walczak

Institute of Experimental Physics, Faculty of Physics, University of Warsaw, Warsaw, Poland

P. Bargassa, C. Beirão Da Cruz E Silva, A. Di Francesco, P. Faccioli, B. Galinhas, M. Gallinaro, J. Hollar, N. Leonardo, L. Lloret Iglesias, M.V. Nemallapudi, J. Seixas, G. Strong, O. Toldaiev, D. Vadruccio, J. Varela

Laboratório de Instrumentação e Física Experimental de Partículas, Lisboa, Portugal

S. Afanasiev, P. Bunin, M. Gavrilenko, I. Golutvin, I. Gorbunov, A. Kamenev, V. Karjavin, A. Lanev, A. Malakhov, V. Matveev [34,35], V. Palichik, V. Perelygin, S. Shmatov, S. Shulha, N. Skatchkov, V. Smirnov, N. Voytishin, A. Zarubin

Joint Institute for Nuclear Research, Dubna, Russia

Y. Ivanov, V. Kim [36], E. Kuznetsova [37], P. Levchenko, V. Murzin, V. Oreshkin, I. Smirnov, V. Sulimov, L. Uvarov, S. Vavilov, A. Vorobyev

Petersburg Nuclear Physics Institute, Gatchina (St. Petersburg), Russia

Yu. Andreev, A. Dermenev, S. Gninenko, N. Golubev, A. Karneyeu, M. Kirsanov, N. Krasnikov, A. Pashenkov, D. Tlisov, A. Toropin

Institute for Nuclear Research, Moscow, Russia

V. Epshteyn, V. Gavrilov, N. Lychkovskaya, V. Popov, I. Pozdnyakov, G. Safronov, A. Spiridonov, A. Stepennov, M. Toms, E. Vlasov, A. Zhokin

Institute for Theoretical and Experimental Physics, Moscow, Russia

T. Aushev, A. Bylinkin [35]

Moscow Institute of Physics and Technology, Moscow, Russia

M. Chadeeva [38], P. Parygin, D. Philippov, S. Polikarpov, E. Popova, V. Rusinov

National Research Nuclear University 'Moscow Engineering Physics Institute' (MEPhI), Moscow, Russia

V. Andreev, M. Azarkin [35], I. Dremin [35], M. Kirakosyan [35], A. Terkulov

P.N. Lebedev Physical Institute, Moscow, Russia

A. Baskakov, A. Belyaev, E. Boos, V. Bunichev, M. Dubinin [39], L. Dudko, A. Ershov, A. Gribushin, V. Klyukhin, O. Kodolova, I. Lokhtin, I. Miagkov, S. Obraztsov, S. Petrushanko, V. Savrin

Skobeltsyn Institute of Nuclear Physics, Lomonosov Moscow State University, Moscow, Russia

V. Blinov [40], Y. Skovpen [40], D. Shtol [40]

Novosibirsk State University (NSU), Novosibirsk, Russia

I. Azhgirey, I. Bayshev, S. Bitioukov, D. Elumakhov, V. Kachanov, A. Kalinin, D. Konstantinov, V. Petrov, R. Ryutin, A. Sobol, S. Troshin, N. Tyurin, A. Uzunian, A. Volkov

State Research Center of Russian Federation, Institute for High Energy Physics, Protvino, Russia

P. Adzic [41], P. Cirkovic, D. Devetak, M. Dordevic, J. Milosevic, V. Rekovic

University of Belgrade, Faculty of Physics and Vinca Institute of Nuclear Sciences, Belgrade, Serbia

J. Alcaraz Maestre, M. Barrio Luna, M. Cerrada, N. Colino, B. De La Cruz, A. Delgado Peris, A. Escalante Del Valle, C. Fernandez Bedoya, J.P. Fernández Ramos, J. Flix, M.C. Fouz, P. Garcia-Abia, O. Gonzalez Lopez, S. Goy Lopez, J.M. Hernandez, M.I. Josa, D. Moran, A. Pérez-Calero Yzquierdo, J. Puerta Pelayo, A. Quintario Olmeda, I. Redondo, L. Romero, M.S. Soares, A. Álvarez Fernández

Centro de Investigaciones Energéticas Medioambientales y Tecnológicas (CIEMAT), Madrid, Spain

J.F. de Trocóniz, M. Missiroli

Universidad Autónoma de Madrid, Madrid, Spain

J. Cuevas, C. Erice, J. Fernandez Menendez, I. Gonzalez Caballero, J.R. González Fernández, E. Palencia Cortezon, S. Sanchez Cruz, P. Vischia, J.M. Vizan Garcia

Universidad de Oviedo, Oviedo, Spain

I.J. Cabrillo, A. Calderon, B. Chazin Quero, E. Curras, J. Duarte Campderros, M. Fernandez, J. Garcia-Ferrero, G. Gomez, A. Lopez Virto, J. Marco, C. Martinez Rivero, P. Martinez Ruiz del Arbol, F. Matorras, J. Piedra Gomez, T. Rodrigo, A. Ruiz-Jimeno, L. Scodellaro, N. Trevisani, I. Vila, R. Vilar Cortabitarte

Instituto de Física de Cantabria (IFCA), CSIC-Universidad de Cantabria, Santander, Spain

D. Abbaneo, E. Auffray, P. Baillon, A.H. Ball, D. Barney, M. Bianco, P. Bloch, A. Bocci, C. Botta, T. Camporesi, R. Castello, M. Cepeda, G. Cerminara, E. Chapon, Y. Chen, D. d'Enterria, A. Dabrowski, V. Daponte, A. David, M. De Gruttola, A. De Roeck, M. Dobson, B. Dorney, T. du Pree, M. Dünser, N. Dupont, A. Elliott-Peisert, P. Everaerts, F. Fallavollita, G. Franzoni, J. Fulcher, W. Funk, D. Gigi, A. Gilbert, K. Gill, F. Glege, D. Gulhan, P. Harris, J. Hegeman, V. Innocente, P. Janot, O. Karacheban [16], J. Kieseler, H. Kirschenmann, V. Knünz, A. Kornmayer [13], M.J. Kortelainen, M. Krammer [1], C. Lange, P. Lecoq, C. Lourenço, M.T. Lucchini, L. Malgeri, M. Mannelli, A. Martelli, F. Meijers, J.A. Merlin, S. Mersi, E. Meschi, P. Milenovic [42], F. Moortgat, M. Mulders, H. Neugebauer, J. Ngadiuba, S. Orfanelli, L. Orsini, L. Pape, E. Perez, M. Peruzzi, A. Petrilli, G. Petrucciani, A. Pfeiffer, M. Pierini, A. Racz, T. Reis, G. Rolandi [43], M. Rovere, H. Sakulin, C. Schäfer, C. Schwick, M. Seidel, M. Selvaggi, A. Sharma, P. Silva, P. Sphicas [44], A. Stakia, J. Steggemann, M. Stoye, M. Tosi, D. Treille, A. Triossi, A. Tsirou, V. Veckalns [45], M. Verweij, W.D. Zeuner

CERN, European Organization for Nuclear Research, Geneva, Switzerland

W. Bertl [†], L. Caminada [46], K. Deiters, W. Erdmann, R. Horisberger, Q. Ingram, H.C. Kaestli, D. Kotlinski, U. Langenegger, T. Rohe, S.A. Wiederkehr

Paul Scherrer Institut, Villigen, Switzerland

L. Bäni, P. Berger, L. Bianchini, B. Casal, G. Dissertori, M. Dittmar, M. Donegà, C. Grab, C. Heidegger, D. Hits, J. Hoss, G. Kasieczka, T. Klijnsma, W. Lustermann, B. Mangano, M. Marionneau, M.T. Meinhard, D. Meister, F. Micheli, P. Musella, F. Nessi-Tedaldi, F. Pandolfi, J. Pata, F. Pauss, G. Perrin, L. Perrozzi, M. Quittnat, M. Reichmann, M. Schönenberger, L. Shchutska, V.R. Tavolaro, K. Theofilatos, M.L. Vesterbacka Olsson, R. Wallny, D.H. Zhu

Institute for Particle Physics, ETH Zurich, Zurich, Switzerland

T.K. Aarrestad, C. Amsler [47], M.F. Canelli, A. De Cosa, R. Del Burgo, S. Donato, C. Galloni, T. Hreus, B. Kilminster, D. Pinna, G. Rauco, P. Robmann, D. Salerno, C. Seitz, Y. Takahashi, A. Zucchetta

Universität Zürich, Zurich, Switzerland

V. Candelise, T.H. Doan, Sh. Jain, R. Khurana, C.M. Kuo, W. Lin, A. Pozdnyakov, S.S. Yu

National Central University, Chung-Li, Taiwan

Arun Kumar, P. Chang, Y. Chao, K.F. Chen, P.H. Chen, F. Fiori, Y. Hsiung, Y.F. Liu, R.-S. Lu, E. Paganis, A. Psallidas, A. Steen, J.f. Tsai

National Taiwan University (NTU), Taipei, Taiwan

B. Asavapibhop, K. Kovitanggoon, G. Singh, N. Srimanobhas

Chulalongkorn University, Faculty of Science, Department of Physics, Bangkok, Thailand

F. Boran, S. Cerci [48], S. Damarseckin, Z.S. Demiroglu, C. Dozen, I. Dumanoglu, S. Girgis, G. Gokbulut, Y. Guler, I. Hos [49], E.E. Kangal [50], O. Kara, A. Kayis Topaksu, U. Kiminsu, M. Oglakci, G. Onengut [51], K. Ozdemir [52], D. Sunar Cerci [48], B. Tali [48], S. Turkcapar, I.S. Zorbakir, C. Zorbilmez

Çukurova University, Physics Department, Science and Art Faculty, Adana, Turkey

B. Bilin, G. Karapinar [53], K. Ocalan [54], M. Yalvac, M. Zeyrek

Middle East Technical University, Physics Department, Ankara, Turkey

E. Gülmez, M. Kaya [55], O. Kaya [56], S. Tekten, E.A. Yetkin [57]

Bogazici University, Istanbul, Turkey

M.N. Agaras, S. Atay, A. Cakir, K. Cankocak

Istanbul Technical University, Istanbul, Turkey

B. Grynyov

Institute for Scintillation Materials of National Academy of Science of Ukraine, Kharkov, Ukraine

L. Levchuk

National Scientific Center, Kharkov Institute of Physics and Technology, Kharkov, Ukraine

R. Aggleton, F. Ball, L. Beck, J.J. Brooke, D. Burns, E. Clement, D. Cussans, O. Davignon, H. Flacher, J. Goldstein, M. Grimes, G.P. Heath, H.F. Heath, J. Jacob, L. Kreczko, C. Lucas, D.M. Newbold [58], S. Paramesvaran, A. Poll, T. Sakuma, S. Seif El Nasr-storey, D. Smith, V.J. Smith

University of Bristol, Bristol, United Kingdom

K.W. Bell, A. Belyaev [59], C. Brew, R.M. Brown, L. Calligaris, D. Cieri, D.J.A. Cockerill, J.A. Coughlan, K. Harder, S. Harper, E. Olaiya, D. Petyt, C.H. Shepherd-Themistocleous, A. Thea, I.R. Tomalin, T. Williams

Rutherford Appleton Laboratory, Didcot, United Kingdom

G. Auzinger, R. Bainbridge, J. Borg, S. Breeze, O. Buchmuller, A. Bundock, S. Casasso, M. Citron, D. Colling, L. Corpe, P. Dauncey, G. Davies, A. De Wit, M. Della Negra, R. Di Maria, A. Elwood, Y. Haddad, G. Hall, G. Iles, T. James, R. Lane, C. Laner, L. Lyons, A.-M. Magnan, S. Malik, L. Mastrolorenzo, T. Matsushita, J. Nash, A. Nikitenko [6], V. Palladino, M. Pesaresi, D.M. Raymond, A. Richards, A. Rose, E. Scott, C. Seez, A. Shtipliyski, S. Summers, A. Tapper, K. Uchida, M. Vazquez Acosta [60], T. Virdee [13], N. Wardle, D. Winterbottom, J. Wright, S.C. Zenz

Imperial College, London, United Kingdom

J.E. Cole, P.R. Hobson, A. Khan, P. Kyberd, I.D. Reid, P. Symonds, L. Teodorescu, M. Turner

Brunel University, Uxbridge, United Kingdom

A. Borzou, K. Call, J. Dittmann, K. Hatakeyama, H. Liu, N. Pastika, C. Smith

Baylor University, Waco, USA

R. Bartek, A. Dominguez

Catholic University of America, Washington DC, USA

A. Buccilli, S.I. Cooper, C. Henderson, P. Rumerio, C. West

The University of Alabama, Tuscaloosa, USA

D. Arcaro, A. Avetisyan, T. Bose, D. Gastler, D. Rankin, C. Richardson, J. Rohlf, L. Sulak, D. Zou

Boston University, Boston, USA

G. Benelli, D. Cutts, A. Garabedian, J. Hakala, U. Heintz, J.M. Hogan, K.H.M. Kwok, E. Laird, G. Landsberg, Z. Mao, M. Narain, J. Pazzini, S. Piperov, S. Sagir, R. Syarif, D. Yu

Brown University, Providence, USA

R. Band, C. Brainerd, D. Burns, M. Calderon De La Barca Sanchez, M. Chertok, J. Conway, R. Conway, P.T. Cox, R. Erbacher, C. Flores, G. Funk, M. Gardner, W. Ko, R. Lander, C. Mclean, M. Mulhearn, D. Pellett, J. Pilot, S. Shalhout, M. Shi, J. Smith, D. Stolp, K. Tos, M. Tripathi, Z. Wang

University of California, Davis, Davis, USA

M. Bachtis, C. Bravo, R. Cousins, A. Dasgupta, A. Florent, J. Hauser, M. Ignatenko, N. Mccoll, S. Regnard, D. Saltzberg, C. Schnaible, V. Valuev

University of California, Los Angeles, USA

E. Bouvier, K. Burt, R. Clare, J. Ellison, J.W. Gary, S.M.A. Ghiasi Shirazi, G. Hanson, J. Heilman, P. Jandir, E. Kennedy, F. Lacroix, O.R. Long, M. Olmedo Negrete, M.I. Paneva, A. Shrinivas, W. Si, L. Wang, H. Wei, S. Wimpenny, B.R. Yates

University of California, Riverside, Riverside, USA

J.G. Branson, S. Cittolin, M. Derdzinski, R. Gerosa, B. Hashemi, A. Holzner, D. Klein, G. Kole, V. Krutelyov, J. Letts, I. Macneill, M. Masciovecchio, D. Olivito, S. Padhi, M. Pieri, M. Sani, V. Sharma, S. Simon, M. Tadel, A. Vartak, S. Wasserbaech [61], J. Wood, F. Würthwein, A. Yagil, G. Zevi Della Porta

University of California, San Diego, La Jolla, USA

N. Amin, R. Bhandari, J. Bradmiller-Feld, C. Campagnari, A. Dishaw, V. Dutta, M. Franco Sevilla, C. George, F. Golf, L. Gouskos, J. Gran, R. Heller, J. Incandela, S.D. Mullin, A. Ovcharova, H. Qu, J. Richman, D. Stuart, I. Suarez, J. Yoo

University of California, Santa Barbara – Department of Physics, Santa Barbara, USA

D. Anderson, J. Bendavid, A. Bornheim, J.M. Lawhorn, H.B. Newman, T. Nguyen, C. Pena, M. Spiropulu, J.R. Vlimant, S. Xie, Z. Zhang, R.Y. Zhu

California Institute of Technology, Pasadena, USA

M.B. Andrews, T. Ferguson, T. Mudholkar, M. Paulini, J. Russ, M. Sun, H. Vogel, I. Vorobiev, M. Weinberg

Carnegie Mellon University, Pittsburgh, USA

J.P. Cumalat, W.T. Ford, F. Jensen, A. Johnson, M. Krohn, S. Leontsinis, T. Mulholland, K. Stenson, S.R. Wagner

University of Colorado Boulder, Boulder, USA

J. Alexander, J. Chaves, J. Chu, S. Dittmer, K. Mcdermott, N. Mirman, J.R. Patterson, A. Rinkevicius, A. Ryd, L. Skinnari, L. Soffi, S.M. Tan, Z. Tao, J. Thom, J. Tucker, P. Wittich, M. Zientek

Cornell University, Ithaca, USA

S. Abdullin, M. Albrow, M. Alyari, G. Apollinari, A. Apresyan, A. Apyan, S. Banerjee, L.A.T. Bauerdick, A. Beretvas, J. Berryhill, P.C. Bhat, G. Bolla [†], K. Burkett, J.N. Butler, A. Canepa, G.B. Cerati, H.W.K. Cheung, F. Chlebana, M. Cremonesi, J. Duarte, V.D. Elvira, J. Freeman, Z. Gecse, E. Gottschalk, L. Gray, D. Green, S. Grünendahl, O. Gutsche, R.M. Harris, S. Hasegawa, J. Hirschauer, Z. Hu, B. Jayatilaka, S. Jindariani, M. Johnson, U. Joshi, B. Klima, B. Kreis, S. Lammel, D. Lincoln, R. Lipton, M. Liu, T. Liu, R. Lopes De Sá, J. Lykken, K. Maeshima, N. Magini, J.M. Marraffino, S. Maruyama, D. Mason, P. McBride, P. Merkel, S. Mrenna, S. Nahn, V. O'Dell, K. Pedro, O. Prokofyev, G. Rakness, L. Ristori, B. Schneider, E. Sexton-Kennedy, A. Soha, W.J. Spalding, L. Spiegel, S. Stoynev, J. Strait, N. Strobbe, L. Taylor, S. Tkaczyk, N.V. Tran, L. Uplegger, E.W. Vaandering, C. Vernieri, M. Verzocchi, R. Vidal, M. Wang, H.A. Weber, A. Whitbeck

Fermi National Accelerator Laboratory, Batavia, USA

D. Acosta, P. Avery, P. Bortignon, D. Bourilkov, A. Brinkerhoff, A. Carnes, M. Carver, D. Curry, R.D. Field, I.K. Furic, J. Konigsberg, A. Korytov, K. Kotov, P. Ma, K. Matchev, H. Mei, G. Mitselmakher, D. Rank, D. Sperka, N. Terentyev, L. Thomas, J. Wang, S. Wang, J. Yelton

University of Florida, Gainesville, USA

Y.R. Joshi, S. Linn, P. Markowitz, J.L. Rodriguez

Florida International University, Miami, USA

A. Ackert, T. Adams, A. Askew, S. Hagopian, V. Hagopian, K.F. Johnson, T. Kolberg, G. Martinez, T. Perry, H. Prosper, A. Saha, A. Santra, V. Sharma, R. Yohay

Florida State University, Tallahassee, USA

M.M. Baarmand, V. Bhopatkar, S. Colafranceschi, M. Hohlmann, D. Noonan, T. Roy, F. Yumiceva

Florida Institute of Technology, Melbourne, USA

M.R. Adams, L. Apanasevich, D. Berry, R.R. Betts, R. Cavanaugh, X. Chen, O. Evdokimov, C.E. Gerber, D.A. Hangal, D.J. Hofman, K. Jung, J. Kamin, I.D. Sandoval Gonzalez, M.B. Tonjes, H. Trauger, N. Varelas, H. Wang, Z. Wu, J. Zhang

University of Illinois at Chicago (UIC), Chicago, USA

B. Bilki [62], W. Clarida, K. Dilsiz [63], S. Durgut, R.P. Gandrajula, M. Haytmyradov, V. Khristenko, J.-P. Merlo, H. Mermerkaya [64], A. Mestvirishvili, A. Moeller, J. Nachtman, H. Ogul [65], Y. Onel, F. Ozok [66], A. Penzo, C. Snyder, E. Tiras, J. Wetzel, K. Yi

The University of Iowa, Iowa City, USA

B. Blumenfeld, A. Cocoros, N. Eminizer, D. Fehling, L. Feng, A.V. Gritsan, P. Maksimovic, J. Roskes, U. Sarica, M. Swartz, M. Xiao, C. You

Johns Hopkins University, Baltimore, USA

A. Al-bataineh, P. Baringer, A. Bean, S. Boren, J. Bowen, J. Castle, S. Khalil, A. Kropivnitskaya, D. Majumder, W. Mcbrayer, M. Murray, C. Royon, S. Sanders, E. Schmitz, J.D. Tapia Takaki, Q. Wang

The University of Kansas, Lawrence, USA

A. Ivanov, K. Kaadze, Y. Maravin, A. Mohammadi, L.K. Saini, N. Skhirtladze, S. Toda

Kansas State University, Manhattan, USA

F. Rebassoo, D. Wright

Lawrence Livermore National Laboratory, Livermore, USA

C. Anelli, A. Baden, O. Baron, A. Belloni, B. Calvert, S.C. Eno, C. Ferraioli, N.J. Hadley, S. Jabeen, G.Y. Jeng, R.G. Kellogg, J. Kunkle, A.C. Mignerey, F. Ricci-Tam, Y.H. Shin, A. Skuja, S.C. Tonwar

University of Maryland, College Park, USA

D. Abercrombie, B. Allen, V. Azzolini, R. Barbieri, A. Baty, R. Bi, S. Brandt, W. Busza, I.A. Cali, M. D'Alfonso, Z. Demiragli, G. Gomez Ceballos, M. Goncharov, D. Hsu, Y. Iiyama, G.M. Innocenti, M. Klute, D. Kovalskyi, Y.S. Lai, Y.-J. Lee, A. Levin, P.D. Luckey, B. Maier, A.C. Marini, C. Mcginn, C. Mironov, S. Narayanan, X. Niu, C. Paus, C. Roland, G. Roland, J. Salfeld-Nebgen, G.S.F. Stephans, K. Tatar, D. Velicanu, J. Wang, T.W. Wang, B. Wyslouch

Massachusetts Institute of Technology, Cambridge, USA

A.C. Benvenuti, R.M. Chatterjee, A. Evans, P. Hansen, S. Kalafut, Y. Kubota, Z. Lesko, J. Mans, S. Nourbakhsh, N. Ruckstuhl, R. Rusack, J. Turkewitz

University of Minnesota, Minneapolis, USA

J.G. Acosta, S. Oliveros

University of Mississippi, Oxford, USA

E. Avdeeva, K. Bloom, D.R. Claes, C. Fangmeier, R. Gonzalez Suarez, R. Kamalieddin, I. Kravchenko, J. Monroy, J.E. Siado, G.R. Snow, B. Stieger

University of Nebraska-Lincoln, Lincoln, USA

J. Dolen, A. Godshalk, C. Harrington, I. Iashvili, D. Nguyen, A. Parker, S. Rappoccio, B. Roozbahani

State University of New York at Buffalo, Buffalo, USA

G. Alverson, E. Barberis, A. Hortiangtham, A. Massironi, D.M. Morse, D. Nash, T. Orimoto, R. Teixeira De Lima, D. Trocino, D. Wood

Northeastern University, Boston, USA

S. Bhattacharya, O. Charaf, K.A. Hahn, N. Mucia, N. Odell, B. Pollack, M.H. Schmitt, K. Sung, M. Trovato, M. Velasco

Northwestern University, Evanston, USA

N. Dev, M. Hildreth, K. Hurtado Anampa, C. Jessop, D.J. Karmgard, N. Kellams, K. Lannon, N. Loukas, N. Marinelli, F. Meng, C. Mueller, Y. Musienko [34], M. Planer, A. Reinsvold, R. Ruchti, G. Smith, S. Taroni, M. Wayne, M. Wolf, A. Woodard

University of Notre Dame, Notre Dame, USA

J. Alimena, L. Antonelli, B. Bylsma, L.S. Durkin, S. Flowers, B. Francis, A. Hart, C. Hill, W. Ji, B. Liu, W. Luo, D. Puigh, B.L. Winer, H.W. Wulsin

The Ohio State University, Columbus, USA

S. Cooperstein, O. Driga, P. Elmer, J. Hardenbrook, P. Hebda, S. Higginbotham, D. Lange, J. Luo, D. Marlow, K. Mei, I. Ojalvo, J. Olsen, C. Palmer, P. Piroué, D. Stickland, C. Tully

Princeton University, Princeton, USA

S. Malik, S. Norberg

University of Puerto Rico, Mayaguez, USA

A. Barker, V.E. Barnes, S. Das, S. Folgueras, L. Gutay, M.K. Jha, M. Jones, A.W. Jung, A. Khatiwada, D.H. Miller, N. Neumeister, C.C. Peng, J.F. Schulte, J. Sun, F. Wang, W. Xie

Purdue University, West Lafayette, USA

T. Cheng, N. Parashar, J. Stupak

Purdue University Northwest, Hammond, USA

A. Adair, B. Akgun, Z. Chen, K.M. Ecklund, F.J.M. Geurts, M. Guilbaud, W. Li, B. Michlin, M. Northup, B.P. Padley, J. Roberts, J. Rorie, Z. Tu, J. Zabel

Rice University, Houston, USA

A. Bodek, P. de Barbaro, R. Demina, Y.t. Duh, T. Ferbel, M. Galanti, A. Garcia-Bellido, J. Han, O. Hindrichs, A. Khukhunaishvili, K.H. Lo, P. Tan, M. Verzetti

University of Rochester, Rochester, USA

R. Ciesielski, K. Goulianos, C. Mesropian

The Rockefeller University, New York, USA

A. Agapitos, J.P. Chou, Y. Gershtein, T.A. Gómez Espinosa, E. Halkiadakis, M. Heindl, E. Hughes, S. Kaplan, R. Kunnawalkam Elayavalli, S. Kyriacou, A. Lath, R. Montalvo, K. Nash, M. Osherson, H. Saka, S. Salur, S. Schnetzer, D. Sheffield, S. Somalwar, R. Stone, S. Thomas, P. Thomassen, M. Walker

Rutgers, The State University of New Jersey, Piscataway, USA

A.G. Delannoy, M. Foerster, J. Heideman, G. Riley, K. Rose, S. Spanier, K. Thapa

University of Tennessee, Knoxville, USA

O. Bouhali [67], A. Castaneda Hernandez [67], A. Celik, M. Dalchenko, M. De Mattia, A. Delgado, S. Dildick, R. Eusebi, J. Gilmore, T. Huang, T. Kamon [68], R. Mueller, Y. Pakhotin, R. Patel, A. Perloff, L. Perniè, D. Rathjens, A. Safonov, A. Tatarinov, K.A. Ulmer

Texas A&M University, College Station, USA

N. Akchurin, J. Damgov, F. De Guio, P.R. Dudero, J. Faulkner, E. Gurpinar, S. Kunori, K. Lamichhane, S.W. Lee, T. Libeiro, T. Peltola, S. Undleeb, I. Volobouev, Z. Wang

Texas Tech University, Lubbock, USA

S. Greene, A. Gurrola, R. Janjam, W. Johns, C. Maguire, A. Melo, H. Ni, K. Padeken, P. Sheldon, S. Tuo, J. Velkovska, Q. Xu

Vanderbilt University, Nashville, USA

M.W. Arenton, P. Barria, B. Cox, R. Hirosky, M. Joyce, A. Ledovskoy, H. Li, C. Neu, T. Sinthuprasith, Y. Wang, E. Wolfe, F. Xia

University of Virginia, Charlottesville, USA

R. Harr, P.E. Karchin, J. Sturdy, S. Zaleski

Wayne State University, Detroit, USA

M. Brodski, J. Buchanan, C. Caillol, S. Dasu, L. Dodd, S. Duric, B. Gomber, M. Grothe, M. Herndon, A. Hervé, U. Hussain, P. Klabbers, A. Lanaro, A. Levine, K. Long, R. Loveless, G.A. Pierro, G. Polese, T. Ruggles, A. Savin, N. Smith, W.H. Smith, D. Taylor, N. Woods

University of Wisconsin – Madison, Madison, WI, USA

[†] Deceased.
[1] Also at Vienna University of Technology, Vienna, Austria.
[2] Also at State Key Laboratory of Nuclear Physics and Technology, Peking University, Beijing, China.
[3] Also at Universidade Estadual de Campinas, Campinas, Brazil.
[4] Also at Universidade Federal de Pelotas, Pelotas, Brazil.
[5] Also at Université Libre de Bruxelles, Bruxelles, Belgium.
[6] Also at Institute for Theoretical and Experimental Physics, Moscow, Russia.
[7] Also at Joint Institute for Nuclear Research, Dubna, Russia.
[8] Also at Suez University, Suez, Egypt.
[9] Now at British University in Egypt, Cairo, Egypt.
[10] Now at Helwan University, Cairo, Egypt.
[11] Also at Université de Haute Alsace, Mulhouse, France.
[12] Also at Skobeltsyn Institute of Nuclear Physics, Lomonosov Moscow State University, Moscow, Russia.
[13] Also at CERN, European Organization for Nuclear Research, Geneva, Switzerland.
[14] Also at RWTH Aachen University, III. Physikalisches Institut A, Aachen, Germany.
[15] Also at University of Hamburg, Hamburg, Germany.
[16] Also at Brandenburg University of Technology, Cottbus, Germany.
[17] Also at MTA-ELTE Lendület CMS Particle and Nuclear Physics Group, Eötvös Loránd University, Budapest, Hungary.
[18] Also at Institute of Nuclear Research ATOMKI, Debrecen, Hungary.
[19] Also at Institute of Physics, University of Debrecen, Debrecen, Hungary.
[20] Also at Indian Institute of Technology Bhubaneswar, Bhubaneswar, India.
[21] Also at Institute of Physics, Bhubaneswar, India.
[22] Also at University of Visva-Bharati, Santiniketan, India.
[23] Also at University of Ruhuna, Matara, Sri Lanka.
[24] Also at Isfahan University of Technology, Isfahan, Iran.

[25] Also at Yazd University, Yazd, Iran.

[26] Also at Plasma Physics Research Center, Science and Research Branch, Islamic Azad University, Tehran, Iran.

[27] Also at Università degli Studi di Siena, Siena, Italy.

[28] Also at INFN Sezione di Milano-Bicocca; Università di Milano-Bicocca, Milano, Italy.

[29] Also at Purdue University, West Lafayette, USA.

[30] Also at International Islamic University of Malaysia, Kuala Lumpur, Malaysia.

[31] Also at Malaysian Nuclear Agency, MOSTI, Kajang, Malaysia.

[32] Also at Consejo Nacional de Ciencia y Tecnología, Mexico city, Mexico.

[33] Also at Warsaw University of Technology, Institute of Electronic Systems, Warsaw, Poland.

[34] Also at Institute for Nuclear Research, Moscow, Russia.

[35] Now at National Research Nuclear University 'Moscow Engineering Physics Institute' (MEPhI), Moscow, Russia.

[36] Also at St. Petersburg State Polytechnical University, St. Petersburg, Russia.

[37] Also at University of Florida, Gainesville, USA.

[38] Also at P.N. Lebedev Physical Institute, Moscow, Russia.

[39] Also at California Institute of Technology, Pasadena, USA.

[40] Also at Budker Institute of Nuclear Physics, Novosibirsk, Russia.

[41] Also at Faculty of Physics, University of Belgrade, Belgrade, Serbia.

[42] Also at University of Belgrade, Faculty of Physics and Vinca Institute of Nuclear Sciences, Belgrade, Serbia.

[43] Also at Scuola Normale e Sezione dell'INFN, Pisa, Italy.

[44] Also at National and Kapodistrian University of Athens, Athens, Greece.

[45] Also at Riga Technical University, Riga, Latvia.

[46] Also at Universität Zürich, Zurich, Switzerland.

[47] Also at Stefan Meyer Institute for Subatomic Physics (SMI), Vienna, Austria.

[48] Also at Adiyaman University, Adiyaman, Turkey.

[49] Also at Istanbul Aydin University, Istanbul, Turkey.

[50] Also at Mersin University, Mersin, Turkey.

[51] Also at Cag University, Mersin, Turkey.

[52] Also at Piri Reis University, Istanbul, Turkey.

[53] Also at Izmir Institute of Technology, Izmir, Turkey.

[54] Also at Necmettin Erbakan University, Konya, Turkey.

[55] Also at Marmara University, Istanbul, Turkey.

[56] Also at Kafkas University, Kars, Turkey.

[57] Also at Istanbul Bilgi University, Istanbul, Turkey.

[58] Also at Rutherford Appleton Laboratory, Didcot, United Kingdom.

[59] Also at School of Physics and Astronomy, University of Southampton, Southampton, United Kingdom.

[60] Also at Instituto de Astrofísica de Canarias, La Laguna, Spain.

[61] Also at Utah Valley University, Orem, USA.

[62] Also at Beykent University, Istanbul, Turkey.

[63] Also at Bingol University, Bingol, Turkey.

[64] Also at Erzincan University, Erzincan, Turkey.

[65] Also at Sinop University, Sinop, Turkey.

[66] Also at Mimar Sinan University, Istanbul, Istanbul, Turkey.

[67] Also at Texas A&M University at Qatar, Doha, Qatar.

[68] Also at Kyungpook National University, Daegu, Korea.